

Matteo Luisi, BSc

Characterizing the measurement
uncertainty of a high-temperature heat
flux differential scanning calorimeter

MASTER THESIS

For obtaining the academic degree
Diplom-Ingenieur

Master Programme of
Technical Physics



Graz University of Technology

Supervisor:

Ao.Univ.-Prof. Dipl.-Ing. Dr.techn. Gernot Pottlacher
Institute of Experimental Physics

Graz, February 2014

Deutsche Fassung:
Beschluss der Curricula-Kommission für Bachelor-, Master- und Diplomstudien vom 10.11.2008
Genehmigung des Senates am 1.12.2008

EIDESSTÄTTLICHE ERKLÄRUNG

Ich erkläre an Eides statt, dass ich die vorliegende Arbeit selbstständig verfasst, andere als die angegebenen Quellen/Hilfsmittel nicht benutzt, und die den benutzten Quellen wörtlich und inhaltlich entnommenen Stellen als solche kenntlich gemacht habe.

Graz, am 17.2.2014.....


.....
(Unterschrift)

Englische Fassung:

STATUTORY DECLARATION

I declare that I have authored this thesis independently, that I have not used other than the declared sources / resources, and that I have explicitly marked all material which has been quoted either literally or by content from the used sources.

02/17/2014
.....
date


.....
(signature)

Abstract

High temperature heat flux differential scanning calorimetry employing various setups and conditions is used to characterize DSC measurement uncertainty at temperatures from 100°C to 1500°C. This work includes uncertainty estimates for temperature and heat calibration, and a complete uncertainty budget for specific heat capacity (c_p) measurements at three given temperatures. It is shown that measurement repeatability is the main factor of influence for determining c_p , accounting for more than 95% of total uncertainty. As repeatability shows substantial variations depending on the crucibles used, a "best-case" scenario is assumed, in which case the overall relative expanded ($k=2$) uncertainty of a sample measurement is 2.1% at 400°C, 2.9% at 800°C, and 4.8% at 1200°C. No significant deviation is found whether platinum crucibles with an Al_2O_3 insert or graphite crucibles are used.

Additionally, the influences of the utilized purge gas and sapphire spacer discs between the probe holder and the crucibles are measured and quantified. Results indicate a substantial decrease of sensitivity in a helium atmosphere as compared to argon, whereas measurement repeatability remains similar. Sapphire spacers only show minor impact on the measured signal and their usage does not significantly affect repeatability.

Kurzfassung

Die Messunsicherheit dynamischer Wärmestromdifferenzkalorimetrie wird mittels zweier Hochtemperaturkalorimeter in einem Temperaturbereich von 100°C bis 1500°C charakterisiert. Diese Arbeit beinhaltet eine Abschätzung der Unsicherheit von Temperatur- und Wärmekalibrierung, sowie ein komplettes Unsicherheitsbudget für Messungen der spezifischen Wärmekapazität c_p bei drei gewählten Temperaturen. Dabei zeigt sich, dass der wichtigste Einflussfaktor auf die Unsicherheit durch die Wiederholbarkeit der Messungen bestimmt ist und auf ihn über 95 % der Gesamtmessunsicherheit entfällt. Da die Wiederholbarkeit für verschiedene Tiegel beträchtlichen Schwankungen unterliegt, wird der Unsicherheitsbestimmung der optimale Fall zugrundegelegt, für den die relative erweiterte ($k=2$) Unsicherheit 2.1 % bei 400°C, 2.9 % bei 800°C und 4.8 % bei 1200°C beträgt. Hierbei werden keine signifikanten Unterschiede zwischen den verwendeten Platintiegeln mit Al_2O_3 -Einsatz und Graphittiegeln festgestellt.

Zusätzlich wird der Einfluss des verwendeten Spülgases, sowie verwendeter Saphirunterlegscheiben zwischen Probenhalter und Tiegeln gemessen und quantitativ ausgewertet. Ergebnisse deuten für Heliumatmosphäre eine erhebliche Abnahme der Empfindlichkeit im Vergleich zu Argon an, während die Wiederholbarkeit ähnlich bleibt. Die Verwendung von Saphirunterlegscheiben zeigt lediglich geringen Einfluss auf das Messsignal und die Wiederholbarkeit.

Contents

1	Introduction	6
2	Differential Scanning Calorimetry	7
2.1	Heat flux DSC setup	7
2.2	Thermodynamic foundations	8
2.3	The baseline	9
2.4	Temperature calibration	10
2.5	Caloric calibration	11
2.6	Sample measurements	12
3	Measurement uncertainty	13
3.1	The GUM view	13
3.1.1	Standard uncertainty evaluation	13
3.1.2	Combined uncertainty evaluation	14
3.1.3	Expanded uncertainty evaluation	15
3.1.4	The central limit theorem	15
3.1.5	Reporting uncertainty	16
3.2	Uncertainty in DSC Measurements	16
3.2.1	Factors influencing measurement uncertainty	17
3.2.2	Uncertainty in temperature measurements	18
3.2.3	Uncertainty in caloric measurements	21
3.2.4	Overview of reported uncertainties	24
4	Experimental validation	25
4.1	Experimental setup	25
4.1.1	DSC 404	25
4.1.2	DSC 404 C Pegasus	26
4.1.3	Purge gas	26
4.1.4	Control system	28
4.2	Working equations	29
4.3	Preparations	30
4.3.1	Crucibles	30
4.3.2	Samples	31
4.4	Temperature calibration	32
4.5	Heat calibration	37
4.6	Heat flow calibration	42
4.7	Repeatability	45
4.7.1	Empty probe holder	46
4.7.2	Pt crucibles with Al ₂ O ₃ inserts	47
4.7.3	Graphite crucibles	50
4.7.4	Reference samples	52
4.7.5	Influence of sapphire spacer discs and purge gas	55

4.7.6	Influence of applied heating rate	57
4.7.7	Influence of working equation	60
4.8	Uncertainty budget	61
4.9	Sources of error	65
4.9.1	Variations in room temperature	65
4.9.2	Defective controller unit power supply	66
4.9.3	Open purge gas inlet valve	66
4.9.4	Purge gas flow variations	66
4.9.5	Bonding between crucibles and probe holder	66
4.9.6	Crucible deformation	67
4.9.7	Sample evaporation	67
4.9.8	Sample oxidation	67
4.9.9	Leakage	68
4.9.10	Supercooling	69
5	Conclusions and outlook	70
6	Acknowledgements	72
	References	73

1 Introduction

Differential Scanning Calorimetry (DSC) describes a thermoanalytical technique measuring enthalpies and heat capacities of various sample materials. It was developed in 1962 and has ever since gained in popularity due to the ability to determine specimen properties over a wide temperature range within a short period of time.

The first heat flux-type differential scanning calorimeter at the Graz University of Technology (TU Graz) was commissioned in 2000 and has been extensively used in several projects. In order to improve the time efficiency of measurements and to be able to re-examine measured results, a second calorimeter was commissioned in early 2013. Both instruments can be utilized at temperatures up to 1500°C and are considered high-temperature calorimeters.

To ensure the quality of a DSC measurement, accurate measurement uncertainty must be provided. However, as opposed to power-compensated DSC, literature data for heat flux DSC uncertainties is scarce, and very little research has been published at temperatures exceeding 800°C. This work aims to give a detailed overview of heat flux DSC uncertainty over a temperature range of 100°C to 1500°C, including a breakdown into individual uncertainty contributions and methods to improve overall uncertainty. The effects of different measurement setups are discussed and quantified, and the experimental results are compared with available published information.

2 Differential Scanning Calorimetry

Differential Scanning Calorimetry (DSC) is a commonly used thermoanalytical technique based on high-precision measurement of heat flux differences. Specifically, the heat flow between a sample and a reference sample is being determined during predefined overall temperature variations (or at a constant temperature) by measuring their temperature difference with the aim of calculating other properties such as the heat capacity of the sample material. Differential Thermal Analysis (DTA) is a technique similar to DSC, however, temperature differences between the sample and the reference are used directly as they fully define the heat flux. DSC was developed in 1962 and first patented by E.S. Watson and M.J. O'Neill under the name "Differential Microcalorimeter" to provide an improved method and apparatus for differential thermal analysis [1]. As DSC use became more common, its techniques were customized and nowadays DSC can be divided into two groups based on different measurement principles - heat flux DSC and power-compensated DSC. Heat flux DSC measures temperature changes between the sample and the reference caused by their difference in enthalpy, whereas power-compensated DSCs measure the power needed to keep the sample and the reference at the same temperature. The following chapter aims to give a quick overview of the functional principle and application of heat flux DSC only. Further information can be found by Hemminger and Cammenga [2], and Höhne et al. [3].

2.1 Heat flux DSC setup

A typical DSC system consists of the sample holder including the heating unit, a temperature control unit, a power unit, and a device to collect measurement data - usually a computer. Additionally, many DSC setups have a vacuum pump as well as a purge gas supply to perform measurements in a defined atmosphere and low-temperature DSC typically includes a cooling system or inlets for liquified gases.

The power and control units follow individual specifications for different DSC setups, but their general functional principle and purpose remains the same - to provide power for the heating unit and control its temperature within strict tolerances.

A schematic of a typical heat flux calorimeter is shown in Fig. 1. It illustrates S , the sample pan, with typical dimensions of about 5 to 8 mm and the reference pan R , located symmetrically to S . Pans can be made of several materials, including aluminium, platinum, and graphite, with the only restriction that their melting temperature must be below the DSC operating temperature. However, it is favorable to choose them in such a way that reactions with both the probe holder and the samples are prevented and diffusion bonding ("sticking") to the probe holder is minimized. Inserts, made of aluminium oxide (Al_2O_3), can be utilized, and lids are common so that heat emission from the sample will not lead to elevated measurement uncertainty. For isobaric operation, lids are slightly perforated.

In order to measure heat flow through sample and reference sample temperatures, thermocouples are attached on the probe holder beneath both pans' contact face (T_S and T_R). The type of thermocouple used depends on the operating temperature range

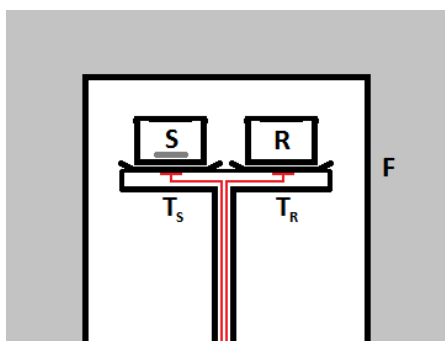


Figure 1: Schematic of a typical heat flux calorimeter. S ... sample pan, R ... reference pan, T_S ... sample thermocouple, T_R ... reference thermocouple, F ... furnace.

of the calorimeter - for high-temperature DSC (using temperatures between 20°C and 1500°C) a type S Pt-Rh thermocouple is common. To ensure good thermal contact and to minimize temperature gradients between the pans and the thermocouple, as well as providing stability and low reactivity at high temperatures, platinum is often used as a material for the contact faces and the surrounding area on the probe holder. High thermal conductivity to the base of the probe holder is, however, not beneficial since it would lead to extended thermal loss and - possibly - interference with the device's electronics. Therefore - and for protection of the thermocouple wires - the connection rod is usually made of a rigid thermal insulator such as aluminium oxide (Al_2O_3).

In Fig. 1, F labels the furnace, the DSC heating unit. Using a thermocouple, the furnace temperature can follow a wide range of temperature programs controlled by the computer. Depending on the type of DSC, the temperature, and the samples measured, the user can choose to apply different heating and cooling rates. Since high-temperature measurements in air can cause oxidation of the samples, an inert gas is typically used to constantly purge the measurement chamber. Typical purge gas flow rates are 20 to 100 ml/min (about 1 to 6 l/h) at an absolute pressure inside the chamber slightly above ambient pressure. A vacuum pump is utilized to remove air before starting the measurement, leading to low overall oxygen content during operation.

2.2 Thermodynamic foundations

The temperature difference ΔT_{SR} measured between the sample pan and the reference pan is connected to the heat flow ϕ by the relation

$$\phi = K(T) \cdot \Delta T_{SR} \quad (1)$$

with the calibration factor $K(T)$ which is found to be dependent on the temperature T . Using calibration materials whose thermodynamic properties are known precisely, $K(T)$ can be determined, making it possible to measure the heat flow rate between the sample and the reference. The total heat Q absorbed or released by the sample during

the measurement is given by ϕ integrated over the time dt .

$$Q = \int_{-\infty}^{\infty} \phi dt \quad (2)$$

According to the first law of thermodynamics, this heat contributes to the differential of the internal energy dU by

$$dU = dQ - p dV \quad (3)$$

with p being the pressure and dV the differential of the volume. Subsequently, the enthalpy H can be introduced, given by

$$dH = dU + p dV + V dp = dQ + V dp \quad (4)$$

Assuming only isobaric changes, the term $V dp$ can be dropped and the heat measured will be equal to the enthalpy change during the measurement. By using this result, the specific heat capacity at constant pressure c_p is found to be

$$c_p = \left(\frac{\partial H}{\partial T} \right) = \frac{dQ}{dT} \quad (5)$$

and can be calculated easily by integrating the measured DSC curve when the calibration factor is known.

2.3 The baseline

DSC measurements can be characterized by the temperature program the sample and the reference are subjected to. Typically for a heat capacity measurement, starting at room temperature or slightly above, a constant heating rate is applied until the required temperature has been reached, followed by a short isothermal segment, and constant-rate cooling back to room temperature. Depending on the sample and the effects to be measured, the heating rate can be varied from 2 K/min to 20 K/min which is the typical range for the instruments used. During cooling, higher rates can be achieved at high temperatures since the device will permit substantial heat loss to the environment. At lower temperatures, instruments without an active cooling system will, however, not be able to cool down as fast due to thermal inertia of the furnace and the lower temperature difference between the environment at room temperature and the device. For example, using a Netzsch DSC 404 C cooling rates of 20 K/min can only be achieved at temperatures exceeding approx. 200°C.

As mentioned above, heat flux between the sample and the reference sample is determined by measuring the temperature difference of the two pans. Using thermocouples, the corresponding signal is an electrical potential difference in the μV range. For typical measurements, the reference sample is an empty pan identical to the sample pan

to minimize measurement contributions caused by the crucibles. Assuming a perfectly symmetrical ideal DSC setup, the signal measured using two empty pans - the so-called baseline - would be zero regardless of the temperature. However, a slightly asymmetrical sample holder placement and other factors of influence - such as unequal thermal contact between the crucibles and the sample holder, or pans of unequal mass - are unavoidable, resulting in a non-zero baseline that varies with heating rate and temperature. Baselines with maximum variations of less than $1\ \mu\text{V}$ are desirable, whereas a poorly set-up device can show variations of $10\ \mu\text{V}$ or more. In order to eliminate this influence when performing measurements, baselines are often recorded beforehand using the same temperature program and then subtracted from the sample measurement signal.

2.4 Temperature calibration

Due to the fact that the thermocouple measuring the sample temperature is located on the probe holder underneath the contact face of the pan, temperatures measured are not exactly equal to the actual sample temperature. Especially when employing high heating rates, the distance and the imperfect thermal connection between the two can lead to temperature differences of several $^{\circ}\text{C}$ [4]. Additionally, the thermocouple itself will not be perfectly calibrated and might show deviations from the actual temperature at the reading point. Both factors can be (at least partially) corrected by temperature calibration.

Temperature calibration is performed by heating calibration substances with well-known melting temperatures above their melting point and recording the resulting DSC curve. Due to the high heat of fusion of the materials used, a large DSC signal (the melting peak) is measured at the respective melting points that can be used to calibrate the thermocouple temperature to the corresponding literary values of the calibration substances. Per definition, the calibration point used is the extrapolated onset of the melting peak since it is independent from the specimen mass and can be determined easily.

If all DSC measurements are to be carried out within a narrow temperature bandwidth, a single calibration point of a suitable calibration material might suffice (one-point calibration) and the resulting temperature difference ΔT between the measurement and the nominal calibration temperature can be added as a constant for all subsequent measurements. For high-precision measurements or measurements across a broader range of temperatures, however, more calibration substances should be utilized. A two-point calibration is done by determining ΔT at two different melting temperatures and using a linear interpolation to expand the calibration to the entire temperature range. Oftentimes, more than two calibration points are used to guarantee high precision at all temperatures.

Common calibration substances for high-temperature DSC are pure metals due to their well-defined melting point and indium (having a melting temperature of 156.6°C) is often used as a reference [5]. At higher temperatures, materials such as aluminium, gold, and nickel can be applied, as well as eutectic systems including Fe-C and Ni-C.

Temperature calibration must be done separately for each heating rate since higher

heating rates will usually lead to a higher temperature difference between the thermocouple and the sample. Calibration during cooling is also possible, however, supercooling of the calibration substances must be considered and corrected for if necessary [6]. Specific guidelines for temperature calibration are provided in ASTM #E967-08 [7].

2.5 Caloric calibration

Caloric calibration is necessary to assign a heat flow rate to the measured DSC signal by using the calibration factor $K(T)$ introduced in equation (1). In DSC several calibration methods can be applied, however, only two are commonly utilized with a regular heat flux DSC: heat calibration by measuring the heat of transition for calibration materials at the respective temperatures, and heat flow calibration by recording the heat flow of a calibration material over a wide temperature range.

Heat calibration uses materials that have well-defined heats of transition (e.g. heat of fusion, or polymorphic transitions) at given temperatures. By measuring the total area under the corresponding DSC signal, a heat Q can be assigned to the transition. If the exact mass of the specimen is known, the measured signal can be compared with the literature value for the calibration substance, and the calibration factor can be calculated at the transition temperature. Similar to temperature calibration, several calibration substances should be used to determine the temperature-dependance of the calibration factor and reduce the uncertainty at temperatures far from calibration points. To minimize other factors of influence, all single calibrations should be performed on the same conditions, especially when determining the heat (the area under the transition curve) from the DSC measurement. Due to baseline variations, however, the onset and the offset of a given transition curve are usually shifted with respect to the abscissa and can not be expected to have the same magnitude, making direct integration infeasible. A simple solution to overcome this problem is to limit the integration to a straight line connecting the onset to the offset. Instead of a straight line, other baseline estimations can be used such as horizontal lines with a cutoff, or sigmoidal connections. More information about peak area determination is provided in ASTM #E2253-08 [8].

In the second approach, heat flow calibration compares the measured heat flow of a calibration substance to its known specific heat capacity c_p across a wide temperature range. Typical calibration materials are synthetic sapphire ($\alpha\text{-Al}_2\text{O}_3$) which can be used at temperatures between 10 and 2250 K and platinum, both showing no sudden variations in c_p at common DSC temperatures [9]. It is preferable to use samples shaped in a way that thermal contact to the pan is maximized (most calibration samples are disc-shaped) with a mass ranging between 10 and 100 mg. For a typical calibration a baseline with the same temperature program is recorded before the measurement of the calibration substance. The resulting calibration curve (calibration measurement minus the baseline) is used to calculate the c_p of the measured specimen (see eq. (5)) which can be compared to its known literary values to determine $K(T)$. Heat flow calibration must be performed separately for each heating rate and - since it requires little time - is sometimes done before each sample measurement to reduce overall uncertainty.

2.6 Sample measurements

In order to analyze sample measurements, characteristic temperatures have to be determined first, often including, but not limited to, the reaction peak's extrapolated onset temperature. Depending on the measurement and the type of specimen utilized, the DSC curve might require "desmearing", effectively minimized deformation of the recorded signal due to thermal lag between the sample and the thermocouple (for more information see [2, 10, 11]). Reaction heats can be found by determining the peak area between the sample measurement and the baseline, and reaction heat flow, often required for kinetic studies, can be analyzed directly from the measured signal. Using Eq. (5), the specific heat of the sample can be calculated.

If possible, the sample mass should be chosen depending on the measurement. Smaller mass will lead to sharp, but small reaction peaks with a well-defined onset temperature and little area, whereas larger sample mass will result in large-area broader peaks due to the longer time it takes for the whole sample to react. Since the pan size is fixed, there is an upper limit to sample size and mass, whereas its lower limit varies depending on the calorimeter's resolution and the desired accuracy. Samples that might react with the crucible material can be analyzed using inserts made of Al_2O_3 , Y_2O_3 , or other nonreactive materials.

3 Measurement uncertainty

Because no measurement of a physical quantity can be exact, its measurement uncertainty is used as an indicator for the quality and reliability of the measurement. Its magnitude depends on the measuring system, the measuring procedure, the skill of the operator, the environment, and other effects [12] and is usually expressed as a non-negative parameter accompanying the result of the quantity measured.

In order to standardize uncertainty evaluation, the "Guide to the expression of uncertainty in measurement" (GUM) [13] was released by the Joint Committee for Guides in Metrology (JCGM) in 1995. Since then, several updates have been published and GUM has been adopted by most major measurement institutes around the world.

3.1 The GUM view

The "Guide to the expression of uncertainty in measurement" (GUM) is intended to serve as an uncertainty evaluation standard in many fields, including quality control, research and development in science and engineering, and development of physical reference standards. The following pages aim to give an overview of the basic concepts and methods used in GUM; for a more thorough explanation see [13].

The term "uncertainty (of measurement)" is defined as a "parameter, associated with the result of the measurement, that characterizes the dispersion of the values that could reasonably be attributed to the measurand" [13, p.2]. Since the experimental result of a measurement is only an estimate of the true value, it must always be accompanied by the uncertainty of the measurement. Traditionally, errors that subsequently attribute to an uncertainty are divided into two components: random and systematic. While random error is due to unknown variations of the result of the measurement and cannot be predicted or compensated for, systematic errors have a more predictable effect on the measurement and can - at least partially - be compensated for by using a correction or correction factor resulting in a zero expectation value of the error. Since the total uncertainty does not only include measurement error but is also influenced by other sources such as incomplete definition of the measurand (the quantity to be measured) or personal bias, GUM distinguishes uncertainty components by method of evaluation rather than by their "random" or "systematic" origin. Type A uncertainty evaluation is performed by statistical analysis of a series of observations, whereas type B evaluation uses alternative methods.

3.1.1 Standard uncertainty evaluation

Given a number of n independent repeated observations q_k of a random variable (fulfilling type A uncertainty evaluation requirements), the corresponding arithmetic mean \bar{q} is usually the best estimate for its expectation value and can be calculated by

$$\bar{q} = \frac{1}{n} \sum_{k=1}^n q_k \quad (6)$$

Due to random effects, single measurements will usually deviate from each other. The resulting variance of the single observations $s^2(q_k)$ is found to be

$$s^2(q_k) = \frac{1}{n-1} \sum_{j=1}^n (q_j - \bar{q})^2 \quad (7)$$

Its positive square root, $s(q_k)$, is the corresponding standard deviation which serves as a parameter to characterize the dispersion of the single observations around \bar{q} . The variance of the mean is

$$s^2(\bar{q}) = \frac{s^2(q_k)}{n} \quad (8)$$

and its positive square root is the standard deviation of the mean, giving a quantitative estimate of the deviation of \bar{q} from the expectation value.

Standard uncertainty of type B is not determined by observation alone, but must be estimated by personal judgement according to its factors of influence. It can be based on data previously taken, personal knowledge and experience with similar measurements, manufacturer's specifications, second-hand uncertainty data, and many others. Even though it can not be calculated directly, it can be as - or more - reliable as type A uncertainty depending on the circumstances. Due to the different origins of type B uncertainty components, a certain number might not be given as standard deviation following a Gaussian distribution. Some uncertainties might exist as multiples of a standard deviation, define a certain level of confidence, or follow other symmetric and asymmetric distribution functions. If necessary, these uncertainties can be converted into single standard deviations for easier comparison or further calculations.

3.1.2 Combined uncertainty evaluation

Often, a measurement result is obtained by observations of more than one input quantity using the functional relationship $y = f(x_1, x_2, \dots, x_i, \dots, x_N)$. In the case where all the variables are unrelated, the combined variance $u_c^2(y)$ can be calculated from the single variances $u^2(x_i)$ by

$$u_c^2(y) = \sum_{i=1}^N \left(\frac{\partial f}{\partial x_i} \right)^2 u^2(x_i) \quad (9)$$

and the combined standard uncertainty is again the positive square root. This equation, based on a first-order Taylor series approximation, can be considered sufficiently precise in most cases. If, however, f is highly non-linear, terms of second order should be added for improved accuracy.

For correlated input quantities, the combined variance is given by

$$u_c^2(y) = \sum_{i=1}^N \sum_{j=1}^N \frac{\partial f}{\partial x_i} \frac{\partial f}{\partial x_j} u(x_i, x_j) \quad (10)$$

or

$$u_c^2(y) = \sum_{i=1}^N \left(\frac{\partial f}{\partial x_i} \right)^2 u^2(x_i) + 2 \sum_{i=1}^N \sum_{j=i+1}^N \frac{\partial f}{\partial x_i} \frac{\partial f}{\partial x_j} u(x_i, x_j) \quad (11)$$

with $u(x_i, x_j)$ being the estimated covariance of x_i and x_j . The correlation between x_i and x_j can be described by the correlation coefficient

$$r(x_i, x_j) = \frac{u(x_i, x_j)}{u(x_i)u(x_j)} \quad (12)$$

3.1.3 Expanded uncertainty evaluation

Per definition, the interval around the measurement result given by the standard uncertainty $u_c(y)$ only encompasses about 68% of all values measured. For some applications, however, it is favoured to provide an uncertainty that includes a larger portion of measurement values. The expanded uncertainty

$$U = k u_c(y) \quad (13)$$

is defined as the combined standard uncertainty multiplied by a coverage factor k . Depending on k , the fraction of measurement values within the interval $y \pm u$ can be modified as required. Common choices are $k=2$, resulting in a 95.4% level of confidence for large sample groups, and - to a lesser extent - $k=3$, resulting in a 99.7% level of confidence.

3.1.4 The central limit theorem

Obtaining precise levels of confidence as mentioned above can be challenging since the experimental standard deviation itself is subject to measurement uncertainty. Its relative standard deviation $\sigma[s(\bar{q})]/\sigma(\bar{q})$ is dependent only on the number of observations n and can be approximated by

$$\sigma[s(\bar{q})]/\sigma(\bar{q}) \approx [2(n-1)]^{-\frac{1}{2}} \quad (14)$$

For $n = 5$, $\sigma[s(\bar{q})]/\sigma(\bar{q})$ is as high as 36% and does not decline quickly - for $n = 10$, it is still 24%, and for $n = 50$, it can be calculated to reach 10%. Therefore, in most cases, distinction between levels of confidence of e.g. 95% (a chance of 1/20 that the value

measured lies outside the interval, corresponding to $k = 1.96$) and 95.4% (for $k = 2$) can not be considered useful.

In order to calculate k , the probability distribution of the measurement result and its corresponding combined standard uncertainty must be known. If all the input quantities X_i follow a normal distribution, the distribution of the result Y will also be normal. Due to the convolution process used to combine the distributions of X_i , however, most of the time Y can be approximated to follow a normal distribution even when many input quantities do not. This behaviour is better known as the Central Limit Theorem.

3.1.5 Reporting uncertainty

In order to ensure measurement results and their corresponding uncertainties are reproducible, sufficient documentation should always be provided. Reports should include a clear description of the methods used to calculate the measurement results and their uncertainties from the observations. Additionally, all uncertainty components should be listed and detailed description of the data analysis should be made available, including all corrections and constants (and their sources).

3.2 Uncertainty in DSC Measurements

Even though DSC has been in use for about fifty years, many publications and reports still lack accurate uncertainty data. This can be attributed to the fact that obtaining trustworthy uncertainties can be challenging and often requires much more work than the actual sample measurement itself. One must not only include the measurement repeatability (which will later prove to be a main factor in determining the total uncertainty), but also the accuracy of the temperature and heat flow calibrations as well as simple basic quantities - such as the specimen mass and its corresponding uncertainty.

Subsequently, many DSCs were often used for order-of-magnitude measurements only, providing qualitative rather than quantitative results. For some applications, such as detecting trace amounts of polyethylene in polypropylene (as mentioned by Richardson [14]), this is perfectly valid of course.

Over the past twenty years, a number of reports have been published which describe ways to minimize errors and uncertainties in DSC measurements and which - for the first time - could conduct precision measurements resulting in total uncertainties of 2 % or less [10, 15, 16]. Under these circumstances DSC can be used in a greater variety of ways that allows it to effectively compete with other calorimetric measurement techniques such as conventional adiabatic calorimetry.

However, there is still very little research regarding DSC measurement uncertainties at temperatures exceeding 800°C. High-temperature DSCs are not as widely used as low- and medium-temperature DSCs as many applications of DSC, such as polymer study, take place at a much lower temperature regime. This can be attributed to a number of reasons, one of which is the more complicated DSC setup. Only a handful of materials can withstand temperatures as high as 1500°C and many of them are not easily processed, such as tungsten which becomes very brittle when constantly exposed

to such high (and higher) temperatures and the sudden temperature changes during each measurement cycle. Other materials utilized are ceramics (which are brittle and do not conduct heat well) and platinum (a good heat conductor, but expensive and it becomes soft at high temperatures). Additionally, the furnace must not only be powerful enough to produce the high temperature required, but must also be able to withstand it during a typical measurement and cool down fast enough - all within very strict tolerances. The higher the temperature, the more important a steady purge gas flow becomes since even trace amounts of oxygen can result in oxidation of certain specimens. All these factors result in high-temperature DSCs being less widespread and, possibly, in higher measurement uncertainties which will be evaluated in chapter 4 (p. 25).

3.2.1 Factors influencing measurement uncertainty

A great number of factors must be considered when calculating the uncertainty of a given DSC measurement, including those for temperature measurements (for example when determining a single melting temperature of an unknown specimen). Some of these can be partially corrected or - at the very least - quantified, whereas others can only be included in the uncertainty calculation by their contribution to the overall repeatability and reproducibility. The following paragraphs aim to present a short overview of basic factors which affect the overall uncertainty and are encountered on a regular basis.

As described in chapter 2.4 (p. 10), temperature calibration should be performed in regular intervals to establish a temperature scale that all subsequent measurements can be based on. Callanan and Sullivan suggest that partial temperature calibration should be repeated daily to minimize temperature uncertainties [17]. If heat flow calibration is necessary, it should also be done in regular intervals.

All DSC measurements are essentially temperature measurements, therefore the thermocouples could be considered the most important parts of the device. Depending on the type of thermocouple and the magnitude of the measurements, its signal-to-noise-ratio must be included in the overall uncertainty budget, as well as possible changes in room temperature (the heat sink end of the thermocouple) during the measurement. Although the thermocouple itself will be calibrated during each temperature calibration, its connection to the crucible (or - in other words - the temperature gradient between the thermocouple and the crucible) can be a major cause for measurement uncertainty [4, 10, 15, 17, 18, 19, 20]. A faulty wiring of the thermocouple has been described by [21] - due to heat expansion the thermocouple wires would come in contact with each other during the heating cycle, leading to sudden apparent crucible temperature changes. Generally speaking, inconsistent thermal contact between the crucibles and the sample holder significantly alters the temperature gradient and thereby increases the uncertainty of the temperature measured. It can be caused by an uneven sample holder surface, an uneven crucible surface and by changing the position of the crucible [15, 18, 22].

The usage of different crucibles and lids will lead to different measurement results [15]. An unequal mass of the two crucibles results in a heat flow from the lighter crucible to the heavier during heating and therefore in a non-zero baseline. Differences in size,

dents, or scratches can change the heat emission/absorption, and Callanan and Sullivan suggest that lids should be flattened if dents are visible [17]. Additionally, incorrect lid placing can add substantial measurement uncertainty as described by Reichelt and Hemminger [23]. Using crucibles made of a different material will usually alter the measurements significantly due to their different heat conductivity, making a new temperature calibration inevitable. Whenever inserts are being used (as described in chapter 2.1, p. 7), their mass and thermal contact with the crucible must also be taken into account.

When setting up the DSC, the sample holder must usually be adjusted to ensure it is placed roughly in the middle of the furnace. Asymmetrical placement inside the furnace will lead to one crucible (and the corresponding thermocouple) being closer to the heating filament than the other, causing a temperature gradient between the crucibles [24]. Hence, the baseline (even if no crucibles are placed on the sample holder) is higher, usually resulting in slightly higher uncertainties.

In most applications, an inert purge gas such as helium, nitrogen, or argon, is used in DSCs to prevent oxidation of the specimen. Since the gas is typically stored at room temperature or below, it will influence the temperature inside the furnace when a steady flow has been established [15]. The attribution to the temperature measured depends on the total flow, the gas' inlet temperature, its heat capacity, and its heat conductivity. Even when high-purity gas and oxygen filters are used, trace amounts of oxygen might result in partial oxidation of certain specimens such as nickel. Depending on the type of specimen used and the extent of oxidation, its heat capacity and/or melting temperature can be significantly different to that of a pure sample. It is therefore recommended to remove oxidation before new measurements are performed [25, 26].

Similar to the thermal gradient between the sample holder and the crucible, a thermal gradient between the crucible and the sample can be detected along with a thermal gradient within the sample [15, 19, 20]. Whereas the thermal gradient within the sample is sometimes neglectable when measuring samples with little mass, the gradient between the crucible and the sample can be significant, depending on the shape of the sample and its contact to the surface [4, 20]. For temperature calibration, melting each specimen once before starting the calibration is an easy solution to minimize this attribution to the overall uncertainty - during the liquid state it will form a certain surface contact with the crucible that will not change significantly after each subsequent melting stage. When operating the calorimeter below the sample's melting temperature, however, the influence of its shape on the measurement uncertainty needs to be considered. Additionally, sample evaporation, possible contamination, and supercooling are other often considerable effects [17, 27].

3.2.2 Uncertainty in temperature measurements

Temperature calibration is an essential task that must be performed before reliable DSC measurements can be taken. In order to conduct an accurate temperature calibration, the calibration materials used must fulfill certain standards (such as high-purity) and, in particular, their melting temperature must be known as precisely as possible. For most pure elements, sufficiently accurate literary values are provided, resulting in melt-

ing temperature uncertainties of less than 0.02°C [15]. At temperatures above 1000°C , however, a smaller number of elements is suitable for temperature calibration since the melting point of the majority of metals lies either below 1000°C or above the maximum temperatures used in DSC. For example, no pure metal suitable for DSC calibration has a melting point between that of copper (1084.6°C) and that of nickel (1454.9°C) [5, 28]. In order to obtain a calibration point in that temperature range, eutectic points of Fe-C (1154°C) or Ni-C (1328°C) can be used [29]. The temperature of these points has not been as accurately specified as the melting temperatures of most pure metals, thus resulting in uncertainties of 0.1°C or more [29]. Therefore, the use of calibration materials such as eutectics should be utilized with caution and the temperature uncertainties must be included in the overall uncertainty budget.

Another source of error is the experimental determination of the melting point using the extrapolated onset of the DSC melting curve (see chapter 2.4, p. 10). Whereas some calibration materials have very well-defined onset points because of their rather linear slope of the melting curve, others can show pre-melting (see [14]) or have uneven slopes that do not permit an exact onset extrapolation.

As discussed in chapter 2.4, guidelines for temperature calibration of DSC and DTA are provided in ASTM #E967-08 [7]. Using indium and zinc as calibration materials to determine the melting point of lead (having a melting temperature intermediate to these), ASTM conducted a multilaboratory study to obtain a measurement uncertainty for the temperature. The standard deviation ($k=1$) of results of the multilaboratory study was estimated to be 0.48°C (reproducibility) as compared to a single-laboratory repeatability of 0.41°C . However, the melting temperatures of indium (156.6°C), zinc (419.5°C), and lead (327.5°C), are far below the maximum operating temperature of high-temperature DSC [5]. Additionally, it remains unknown as to how much uncertainty stems from actual measured temperature deviations from the literary values of the calibration substances, and how much originates from the - possibly inadequate - linear interpolation between the calibration points.

A thorough analysis of the former (among other things) was conducted by Callanan and Sullivan, using a power-compensated DSC at temperatures from -160°C to 580°C and heating rates from 5 K/min to 20 K/min [17]. The standard deviations of melting temperatures at calibration points were found to lie between 0.02°C and 0.10°C at optimal conditions, quite close to the literary value uncertainties and the absolute measurement uncertainty of the thermocouples. Most other research, however, shows repeatability of 0.1°C to 0.4°C at calibration points between 150°C and 700°C , depending on the melting temperature of the specimens and the type of crucible used [4, 15, 16, 18, 25]. Höhne et al. even assume temperature uncertainties between 0.1 and 0.8°C at calibration points [3]. As a general rule, a higher melting temperature typically indicates a higher measurement uncertainty. With a low melting point such as about 156.6°C for indium, the repeatability will most likely be 0.1°C or less, whereas aluminium - which in many cases is the highest calibration point used - will show uncertainties of 0.2°C or more. When increasing the temperature further, research suggests the uncertainty

will grow more rapidly. Trustworthy published uncertainty data, however, is scarce to non-existent for temperatures exceeding 800°C.

In addition to uncertainty originating from repeatability at the calibration points, it can be assumed that a non-marginal influence on the temperature calibration accuracy stems from the interpolation method used. While linear interpolation (or even one-point calibration, resulting in a single constant calibration temperature offset) can surely be efficient at temperatures close to the calibration points, a higher-order interpolation might result in a higher overall accuracy, assuming a sufficient number of calibration points are available. Which interpolation method ultimately provides the most accurate results, however, depends on the DSC setup and can only be found through experimentation. If the number of calibration points exceeds the order of the interpolation, a rough estimation of the temperature uncertainty can be given by analyzing the deviation between the calibration points measured and the interpolated function at the respective temperatures.

As mentioned previously, total temperature repeatability/reproducibility values are made available by ASTM International for temperatures up to around 400°C [7]. A more thorough uncertainty evaluation is provided by Rudtsch [10] - using a power-compensated DSC -, including a breakdown of the temperature uncertainties into $\Delta\theta_{mat}$ - the uncertainty of the melting temperature of the calibration material - , $\Delta\theta_{calib}$ - the uncertainty of the temperature calibration measurements - , $\Delta\theta_{lin}$ - the uncertainty caused by linearisation of the three-point calibration - , and $\Delta\theta_{lag}$ - the uncertainty caused by thermal lag. Respective standard uncertainty values for a temperature measurement at approx. 500°C are 0.1°C, 0.3°C, 0.5°C, and 0.2°C, resulting in a total standard uncertainty of 0.6°C.

The term "thermal lag" used by Rudtsch describes the temperature difference between the instrument and the sample. While direct quantification of this parameter is not feasible since the sample's mean temperature cannot be measured directly, it is possible to determine the thermal lag during the sample measurement if a power-compensated DSC is utilized [30]. In an ideal DSC measurement, the heat flow rate would re-adjust without delay when changing the heating rate. Due to temperature difference between the heater and the sample, however, there will be additional heat flow resulting in an enthalpy change of the sample. Using this enthalpy change, the thermal lag can be quantified and its uncertainty can be included in the overall uncertainty budget. Rudtsch found that the thermal lag is temperature-dependent and slightly decreases with higher temperatures. In the case of heat flux DSC, additional heat contribution from the furnace, however, makes direct calculation of the thermal lag impossible and empirical methods must be applied to approximate its contribution [30]. In order to distinguish the thermal lag of the material from the thermal lag of the instrument used, samples of similar geometry but different thickness can be measured [14]. It is then possible to extrapolate to zero thickness, effectively providing an estimation of the thermal lag of the crucibles and the instrument only.

High-temperature DSC uncertainties are described by Baumann et al. [31] using a heat-flux DSC at temperatures ranging from 1000 to 1300°C. In this case, the temperature uncertainty at the curie point of cobalt at 1123°C was determined to be 15.2°C.

Chapman [32] applies high-temperature DSC to nickel based superalloys at temperatures between 1250°C and 1450°C, resulting in temperature uncertainties of roughly 5°C. Compared to uncertainties of less than 0.5°C often found at temperatures below 700°C, these seem to be increased by one order of magnitude or more.

Some of the factors described in chapter 3.2.1 (p. 17) will cause overall uncertainty to rise substantially with increasing temperature. An example is the influence of temperature gradients within the sample (similar to thermal lag discussed above). Due to the experimental difficulty of measuring these gradients directly, Comesaña et al. analysed a simulated TGA-DSC device at temperatures between 30 and 230°C and it was found that the magnitude of the thermal gradient did not only depend on the specimen and the heating rate, but also on the mean sample temperature [33]. At a furnace temperature of 80°C, the difference between the sample maximum and minimum temperature was approx. 0.2°C which seemed to linearly increase with temperature showing a temperature difference of approx. 0.4°C at 190°C. Assuming the linear relationship is still valid at higher temperatures, this would result in a temperature gradient of up to 2.6°C for high-temperature DSC. Even though this is only a very simplified approximation lacking many influential factors, it shows one of the difficulties of conducting high-precision measurements at high temperatures.

3.2.3 Uncertainty in caloric measurements

As discussed in chapter 2.5 (p. 11), caloric calibration can be performed by measuring the melting enthalpy of a calibration material with a known heat of fusion (enthalpy or heat calibration) limiting the calibration to the corresponding melting temperature points, and by measuring a calibration material (such as synthetic sapphire) across a broad temperature range and comparing the result to its known temperature-dependent heat capacity (heat-flow rate calibration). Due to the systematic difference between the two, Sarge et al. suggest both be carried out in order to measure heat flow rates and reaction heats (such as heat of fusion) accurately [20].

5.2.3.1 Uncertainty in heat calibration

Heat calibration is typically highly precise close to the melting temperatures of the calibration materials since the heat of fusion generates a very large DSC signal, providing an excellent signal-to-noise ratio. Due to the large but narrow melting peak, baseline variations are not a major cause for concern and repeatability is generally favorable. Uncertainties arise due to the accuracy of the literature enthalpy values of the calibration materials, the weighings of the specimens used, the noise in the DSC signal, the experimental determination of the peak area, and the thermal coupling between the sample and the measuring system [20]. Poeßnecker suggests that especially the latter is a major uncertainty contribution due to unavoidable air gaps between the sample holder and the pan [34]. Additionally, similar to temperature calibration, interpolation between calibration points is necessary and thus likely to result in larger overall uncertainties.

Similar to the guidelines for temperature calibration [7], heat flow calibration guidelines are provided by ASTM #E968-02 (Standard Practice for Heat Flow Calibration of Differential Scanning Calorimeters) [35]. Therein, the melting endotherm of a high-purity standard material - in this case, indium - is recorded and integrated to determine the melting enthalpy of the material used. To obtain reliable uncertainty data, the measured heat of fusion was compared with values for lead and zinc, at 327.5°C and 419.5°C respectively. The measurement repeatability at the melting point of indium (156.6°C) has been found to be 0.94%, which was then extended to temperatures within 265°C of this point yielding a repeatability of 1.4%. Per each additional 100°C beyond these limits, repeatability is expected to decrease by 0.7%. The corresponding reproducibility (determined via a multilaboratory study in which 13 laboratories participated) was found to be 2.7% within 265°C of the calibration point, decreasing by 2.0% per each additional 100°C. Extrapolating these findings to high-temperature DSC would lead to unacceptable heat flow calibration reproducibilities of up to 25% when using indium as a single calibration material.

Supplementary enthalpy calibration data is provided by della Gatta et al. for gallium ($T_{melt} = 29.8^\circ\text{C}$), indium ($T_{melt} = 156.6^\circ\text{C}$), and tin ($T_{melt} = 231.9^\circ\text{C}$), showing a repeatability of approx. 1% at the calibration points [15]. Similar results have been obtained by Nieto de Castro et al. [16]. Additionally, the determined calibration factor shows statistically significant differences from approx. 0.8% (for Gallium) to approx. 0.2% (for tin) for different heating rates used. Generally, a low heating rate of 1 K/min resulted in slightly lower calibration factors than the higher heating rates of 5 K/min and 10 K/min. This result is unexpected, since in theory the calibration factor only depends on the heat of fusion (the area of the peak curve), a material constant independent from the applied heating rate.

Analogous to uncertainties in temperature calibration, enthalpy calibration uncertainties seem to increase with temperature. Sarge et al. show uncertainties from 0.2% for indium and 0.3% for tin to 1.2% for aluminium ($T_{melt} = 660.3^\circ\text{C}$) [20]. No reported enthalpy uncertainty data for temperatures exceeding 700°C has been found.

5.2.3.2 Uncertainty in heat flow rate calibration

Heat flow rate calibration accuracy is affected by similar factors as heat calibration, such as uncertainties in the calibration material's mass and heat capacity literature values, the thermal coupling between sample and sample holder, and temperature gradients inside the sample [20]. Temperature uncertainties (see above) must be included, however, the enthalpy of most calibration materials does not substantially change for minor temperature deviations, thereby not causing a significant total uncertainty contribution. Conversely, the repeatability of both calibration sample measurement and baseline measurement can be major influential factors.

Sapphire ($\alpha\text{-Al}_2\text{O}_3$) is one of the most commonly utilized calibration materials, for which high-temperature enthalpy data is provided by Ditmars et al. [9]. Its high melt-

ing temperature and its reproducible enthalpy and heat-capacity values make it highly suitable as a calibration substance at a temperature range from -263°C to 1980°C .

Heat flow calibration uncertainties are provided by Rudtsch using a power-compensated DSC at temperatures between 30°C and 600°C [10]. Measurement repeatability is shown to be approx. 0.5% and is not strongly dependent on temperature, showing only slightly higher uncertainty below 300°C and above 550°C . A relative, overall uncertainty of a (single) heat flow calibration was found to be 0.7% while assuming rectangular probability distribution. Performing a thorough heat flow rate calibration at temperatures ranging from 120°C to 300°C , Sarge et al. suggest a similar uncertainty contribution, beginning from approx. 0.3% for 120°C to approx. 0.7% for 260°C using a corundum (Al_2O_3) sample with a mass of 130 mg [20]. Reducing the sample weight to 7.8 mg increases the uncertainty to approx. 2.1% for 120°C and approx. 1.9% for 260°C .

Baumann et al. performed high-temperature calibration measurements on a Netzsch DSC 404 C at temperatures up to approx. 1200°C using high-purity cobalt and molybdenum as calibration substances [31]. Making use of conventional platinum pans with Y_2O_3 inserts, repeatability data exceeding 5% is reported for consecutive trials. Those results were significantly improved by allowing diffusion bonding of the pans on the sample stage instead of lifting up the pans after each measurement. This suggests that the thermal contact between the sample holder and the crucibles accounts for a large part of the total repeatability.

5.2.3.3 Uncertainty in determining specific heat capacity

ASTM #E968-02 guidelines for determining specific heat capacity by differential scanning calorimetry [36] specify that a heat flow rate calibration is to be performed prior to each sample measurement. The resulting DSC curves are to be compared and by using the known heat capacity of the reference material (sapphire), the unknown specimen's heat capacity can be calculated. An interlaboratory study was conducted by ASTM at DSC temperatures between 40°C and 80°C , and the resulting measurement precision was documented. The standard deviation in a specific heat capacity measurement at 67°C was found to be 2.2% in single laboratory measurements (repeatability) and 3.0% in multilaboratory conditions (reproducibility). The absolute bias (the difference between the mean c_p measured and its corresponding literature value) was found to be less than 1.8% for all measurements, which was well within the measurement repeatability.

Using a power-compensated DSC, Rudtsch provided the uncertainty of specific heat measurements at 250°C [10]. Using a certified sapphire as reference material, total expanded ($k=2$) uncertainties of 1.5% are reported for the specific heat corresponding to a standard deviation of 0.8%. As described before, measurement repeatability is assumed to be the major cause for these uncertainties and - to a lesser extent - thermal lag. Additionally, it is shown that the uncertainty of the specific heat measurement does not appear to be a function of temperature between 0°C and 600°C and is therefore valid across this entire range. Nieto de Castro et al. report the same absolute uncertainty in specific heat capacity measurements for a temperature range of 30°C to 130°C

which is proportional to the uncertainty obtained for temperature and enthalpy measurements [16].

3.2.4 Overview of reported uncertainties

Table 1 shows an overview of uncertainties reported in DSC measurements carried out at different temperature ranges (see column "Temp. [°C]"). If temperature or heat/heat flow uncertainties are provided, it is indicated in columns " $U(T)$ " and " $U(Q|\phi)$ " and, in case total measured heat capacity uncertainty has been calculated, the corresponding values can be found in column " $U(c_p)$ ". Unless otherwise specified, all stated values for $U(c_p)$ match an expanded uncertainty with $k=2$. The column "Budget" denotes if a complete uncertainty budget (see chapter 4.8, p. 61) was reported.

Table 1: Reported uncertainties in DSC measurements. Temp... temperature range, $U(T)$... reported temperature uncertainty, $U(Q|\phi)$... reported heat/heat flow uncertainty, $U(c_p)$... measured heat capacity uncertainty, Budget... reported uncertainty budget.

Reference	Temp. [°C]	$U(T)$	$U(Q \phi)$	$U(c_p)$	Budget
ASTM [7]	150 to 420	yes	no	-	no
ASTM [35]	-130 to 420	no	yes	-	no
ASTM [36]	40 to 80	no	no	6.2 % ^{1,2}	no
Baumann et al. [31]	930 to 1300	yes	yes	-	no
Callanan and Sullivan [17]	-160 to 580	yes	no	0.4 - 0.6 %	no
Cammenga et al. [25]	150 to 660	yes	no	-	no
Chapman [32]	1000 to 1500	yes	no	-	no
Comesaña et al. [33]	30 to 330	yes ³	no	-	no
Della Gatta et al. [15]	-70 to 530	yes	yes	1 - 2 %	no
Hanitzsch [22]	20 to 600	no	no	< 3 %	no
Höhne et al. [18]	30 to 330	yes	no	-	no
Hopkins [37]	20 to 1500	yes	yes	-	no
Malheiro et al. [38]	150 to 330	yes	no	-	no
Nieto de Castro et al. [16]	-100 to 800	yes	yes	< 1.5 % ⁴	no
Richardson [14]	-40 to 690	no	yes	2 % ¹	no
Richardson and Savill [4]	-40 to 690	yes	no	-	no
Rudtsch [10]	0 to 600	yes	yes	1.5 %	yes
Sarge et al. [20]	-200 to 730	no	yes	-	no
Sarge et al. [27]	-170 to 580	no	yes	-	no
Wilthan [21]	200 to 1200	no	no	3 %	no

¹ at calibration points

² for $k = 2.8$

³ using a simulated TGA-DSC device

⁴ at temperatures from 30°C to 130°C

4 Experimental validation

4.1 Experimental setup

All subsequent measurements were performed on two different high temperature differential scanning calorimeters: The Netzsch DSC 404 and the Netzsch DSC 404 C Pegasus. They are controlled by a PC using the Netzsch Proteus software for temperature cycle regulation and data acquisition.

4.1.1 DSC 404

The Netzsch DSC 404, commissioned in 2000, is a high temperature heat flux DSC with a working range between 250°C and 1500°C. It can be divided into: The calorimeter, a power supply unit, and a controller unit which is connected to a PC. Additionally, a manual purge gas supply is used and is described in more detail in chapter 4.1.3 (p. 26).



Figure 2: The Netzsch DSC 404 high temperature heat flux calorimeter

The main measurement unit is shown in Fig. 2. The large metal cylinder houses the furnace and includes an air cooling system to permit rapid heat removal during cooling cycles. It can be manually lifted to allow access to the probe holder, and vacuum tightness is ensured by a rubber seal at the bottom of the furnace. As described in chapter 2.1 (p. 7), the probe holder is located in the center of the furnace and is shown in Fig. 3.

The probe holder consists of an Al_2O_3 rod and a platinum DSC- c_p head on an Al_2O_3 disc. Heat shields on the probe holder provide additional protection from heat loss during measurements. PtRh type S thermocouples are located directly underneath the platinum surface of the head and their wires run within the Al_2O_3 rod towards an attachment plug at the bottom of the probe holder. The position of the probe holder within the



Figure 3: The DSC 404 probe holder with DSC- c_p head

furnace can be adjusted by tightening/loosening three screws located perpendicular to the rod. To prevent material from falling into the circuitry next to the attachment plug when handled carelessly, a metal cover can be inserted between the probe holder and the casing of the DSC.

4.1.2 DSC 404 C Pegasus

Similar to the DSC 404, the Netzsch DSC 404 C Pegasus consists of a calorimeter, a power supply unit, a controller unit, and a purge gas supply. Commissioned in 2013, it is considered a successor of the DSC 404. With the same temperature working range, its advantages are primarily a decreased signal noise, improved baseline behaviour, a reduced influence of ambient conditions, and an automated purge gas supply. The calorimeter and its probe holder can be seen in Fig. 4 and Fig. 5, respectively.

The probe holder features a high accuracy DSC- c_p head made of platinum which - compared to the DSC 404 - has a higher mass and encompasses the majority of the Al_2O_3 disc on top of the rod. Other differences include an automated lifting mechanism for the furnace and easier adjustment of the probe holder by using two micrometer screws instead of three regular screws. Additionally, the calorimeter features an integrated flowmeter to control the purge gas flow rate from up to two inlets by using control knobs on the device.

4.1.3 Purge gas

In order to avoid oxidation of certain specimens during the measurement, a steady flow of an inert purge gas is used to constantly flood the measurement chamber and remove any oxygen from the surrounding atmosphere. It is introduced via feed lines through the insert valve on the back of the calorimeter and exhausted through a pressure valve next to the insert valve (DSC 404) or at the top of the furnace (DSC 404 C) keeping the pressure inside between 0.1 atm and 0.2 atm above ambient pressure. The gases used are



Figure 4: The Netzsch DSC 404 C high temperature heat flux calorimeter



Figure 5: The DSC 404 C probe holder with high accuracy DSC- c_p head

argon 5.0 and helium 5.0 (corresponding to a purity of 99.999 % and an oxygen content of less than 2 ppm). Typically, a flow rate of 100 ml/min is utilized, and is measured with a Brooks Sho-Rate 1355 (DSC 404) and a Vögtlin V-100 (DSC 404 C) glass tube flow meter. Additionally, a Restek RK22020 triple filter is installed between the purge gas inlet and the calorimeter to further remove moisture, hydrocarbons, and oxygen resulting in total gas purity of 6.0 or better.

Before a measurement is started, the pressure inside the measurement chamber is

lowered to approx. 10^{-3} mbar using a rotary vane pump and is subsequently filled with the inert purge gas. This procedure is repeated three times to ensure complete removal of air prior to the measurement. Depending on the type of DSC, the pump and the purge gas flow must be started manually (DSC 404) or can be controlled electronically (DSC 404 C).

4.1.4 Control system

As described above, a computer is used to operate the calorimeter by defining a temperature cycle that the sample and the reference sample should undergo. The user's input is then relayed to the calorimeter by a controller which can access a power unit to provide the power necessary to heat the furnace according to the desired temperature program. The control unit is also used to regulate the purge gas flow for the DSC 404 C. Measurement data from the thermocouples is recorded by the control unit and digitally sent to the computer for acquisition and evaluation.

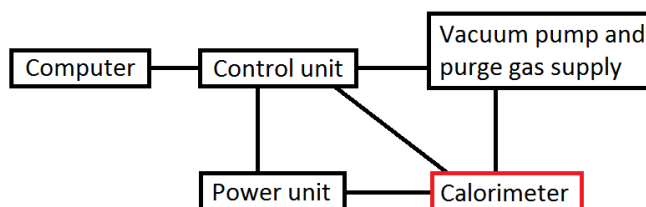


Figure 6: Basic setup of high-temperature DSC components including purge gas supply

Fig. 6 shows the parts of the DSC setup used for this work. The Netzsch Proteus Measurement 6.0.0 software is employed in order to define the measurement cycle and for data acquisition. Its functions include:

- Defining a temperature cycle with variable heating rates
- Enabling/disabling purge gas flow depending on the temperature program section
- Recording DSC data with variable sampling rates
- Enabling emergency shutdown if furnace reaches a user-defined temperature limit
- Storing additional measurement information (e.g. pans used, purge gas type, sample/reference sample information)

Further data evaluation and data export is performed with the Netzsch Proteus Thermal Analysis 6.0.0 software. It can access measurement raw data files created by Netzsch Proteus Measurement and features functions such as:

- Enthalpy and c_p calculation from raw data provided using the ratio method (see chapter 4.2, p. 29)

- Automatic baseline subtraction/correction
- Temperature and heat calibration support including onset temperature determination and peak area calculations
- Data export and visualization

For additional data correction (including a correction method for the working equation, see chapter 4.2) and illustration Origin 8.6 is used.

4.2 Working equations

The measurement signal recorded by the DSC (commonly referred to as the "DSC signal") is a voltage in the μV range which corresponds to the heat flow between the sample pan and the reference sample pan as a function of time or sample temperature. In order to relate the DSC signal to the temperature-dependent heat capacity c_p of a sample, calibrations according to chapter 2.4 (p. 10) and chapter 2.5 (p. 11) must be performed. When a sample without sudden large heats of transition is measured, it is convenient to conduct a heat flow rate calibration during the measurement. This is done by measuring not only the baseline and the sample, but also a reference sample with known c_p using the same crucibles. This procedure results in a very low calibration uncertainty as the environmental conditions should remain similar within the typical measurement timeframe of up to 1.5 days.

The heat capacity $c_{p,S}$ of the sample can then be calculated with the working equation. The ratio of the DSC signals of sample Φ_S and reference sample Φ_R corrected by the baseline Φ_0 must equal the ratio of the specific heat capacities of sample $c_{p,S}$ and reference sample $c_{p,R}$ weighted by their masses m_S and m_R , respectively [39]. This "ratio method" is given by equation (15) below

$$c_{p,S} = \frac{m_R}{m_S} \cdot c_{p,R} \cdot \frac{\Phi_S - \Phi_0}{\Phi_R - \Phi_0} \quad (15)$$

This equation does not account for possible additional uncertainties that contribute to signal shifts at different isothermal temperature segments. Due to the geometry of the DSC setup, a non-zero heat flow will be measured in isothermal mode. However, this additional heat flow is not constant over the whole temperature range and depends on the crucibles as well as the samples and reference samples measured. Therefore, it can not be completely eliminated by just baseline correction. If an isothermal phase is added before and after the heating segment of the measurement, an improved working equation provided in ASTM #E1269-11 can be used by applying a correction factor δ for each measurement to normalize the additional signal offset [36].

$$c_{p,S} = \frac{m_R}{m_S} \cdot c_{p,R} \cdot \frac{(\Phi_S + \delta\Phi_S) - (\Phi_0 + \delta\Phi_0)}{(\Phi_R + \delta\Phi_R) - (\Phi_0 + \delta\Phi_0)} \quad (16)$$

The "ASTM method" and the corresponding correction will subsequently be used for

all uncertainty calculations including repeatability measurements (see chapter 4.7, p. 45) unless mentioned otherwise.

4.3 Preparations

Prior to beginning a measurement, preparatory work must be conducted to ensure a functional working environment. Specifically, the crucibles used for experimental work were carefully selected and partially modified. Sample and reference sample purity were also major concerns since even minimal impurities can significantly alter measurement results. Additionally, the oxygen content of the surrounding atmosphere had to be minimized and kept at a low level during the measurement to avoid specimen oxidation.

4.3.1 Crucibles

Typically, platinum (Pt) crucibles with aluminium oxide (Al_2O_3) inserts were used and purchased from Netzsch. The Pt pans have a cylindrical shape with a flat bottom, measuring 6.8×2.7 mm (diameter \times height) and a material thickness of approx. $80 \mu\text{m}$. The Al_2O_3 inserts - used as a non-reactive container for samples that might react with the Pt crucible - measure 6.5×1.9 mm (d \times h) with a wall thickness of approx. $180 \mu\text{m}$ and fit tightly inside the Pt pans. Due to the fact that aluminium oxide becomes transparent when exposed to high temperatures, the platinum surrounding is necessary to prevent energy loss from radiation during the measurement. A flat platinum lid is placed on top of the crucible to minimize possible sample evaporation and further radiation loss. To prevent large specimens from touching the lid, one lid was slightly curved and is used for samples exceeding a diameter of 2 mm. The Pt+ Al_2O_3 pan combination can be used throughout the entire temperature range covered by the DSC (20°C to 1500°C).

Graphite crucibles and lids without inserts were investigated as a possible alternative to the Pt+ Al_2O_3 combination. With a similar shape, they measure 6.8×4.0 mm (d \times h) and have a wall thickness of approx. $240 \mu\text{m}$. They can also be utilized throughout the entire temperature range, however, usage of sample materials is limited due to the possible reaction and formation of eutectic systems with the graphite.



Figure 7: Pt crucible with Al_2O_3 insert and graphite crucible, including lids

Prior to the first measurement, platinum crucibles and aluminium oxide inserts were cleaned in an ultrasound acetone bath and were subsequently subjected to a heating

cycle reaching 1250°C for extended periods of time to remove remaining surface impurities. They were then weighed using a Mettler Toledo AB104-S-A microbalance with a measurement uncertainty between 0.2 mg and 0.5 mg depending on the specimen mass. The combinations of reference sample pans and sample pans were chosen so that their masses (and total heat capacities) were as similar as possible in order to minimize the baseline signal. Crucibles with visible dents and scratches were discarded.

When conducting measurements with prolonged exposure to high temperatures, Pt crucibles tend to show slight bonding to the probe holder as a result of diffusion processes between the contact surfaces. Depending on the measurement, there is a risk of damaging both the crucibles and the probe holder when removing the pans. Diffusion bonding can be prevented by placing a thin sapphire disc between the probe holder and the crucible. Usage of sapphire spacers measuring 6.8 mm × 75 μm (d × h) purchased from SaphTec is evaluated in chapters 4.4 (p. 32) to 4.7 (p. 45). Sapphire spacers were also used with graphite pans as the coating of the graphite can react with the probe holder thus rendering the pan unusable. See chapter 4.9.5 (p. 66) for more information about sapphire spacer discs. To maximize the contact surface between sample holder (or sapphire spacer discs) and crucibles, the bottoms of Pt pans were flattened using a mechanical press. For more information see chapter 4.9.6 (p. 67).

4.3.2 Samples

A wide range of materials are covered by the samples used in DSC measurements. Whereas reference samples for temperature and heat calibration must feature well-defined phase transitions with high transition enthalpies, reference samples for heat flow calibration ideally show a continuous specific heat capacity without major fluctuations throughout the entire temperature range.

Calibration samples for temperature and heat calibration include metals such as indium, aluminium, gold, and nickel and were provided by Netzsch either in the form of wires or small plates. They were subsequently cut to a suitable size and weighed using a high precision Sartorius MC 5 microbalance with standard measurement uncertainties of less than 10 μg. See chapters 4.4 (p. 32) and 4.5 (p. 37) for a more comprehensive list of temperature and heat calibration materials, their corresponding masses, and uncertainties.

Heat flow calibration was primarily performed using cylindrically-shaped synthetic sapphire (α -Al₂O₃) reference samples with a diameter of approx. 5.8 mm purchased from Netzsch in different masses to ensure a similar heat capacity as the sample specimens. Sapphire samples can be used up to 1800°C for calibration purposes and have a well-defined continuous specific heat capacity. Other reference materials evaluated for heat flow calibration usage include platinum and molybdenum (for more information see chapter 4.6, p. 42).

As sample impurities can significantly alter thermodynamic properties, specimens were cleaned with acetone or isopropanol prior to measurement. Specimens that showed signs of oxidation or other surface reactions were discarded.

4.4 Temperature calibration

As described in chapter 2.4 (p. 10), temperature calibration is necessary to determine the actual sample temperature T_S from the temperature T_m measured by the thermocouple underneath the sample pan. This can be expressed by the relation

$$T_S = T_m + \Delta T(T_m) \quad (17)$$

with a temperature-dependent offset $\Delta T(T_m)$. $\Delta T(T_m)$ can be determined by measuring the extrapolated onset temperature of melting peaks of reference materials and calculating the difference with their respective literature values. Through interpolation, $\Delta T(T_m)$ is then extended to the whole temperature range covered by calibration materials.

Suitable reference materials for temperature calibration are shown below, including their nominal melting temperatures T_{nom} and an estimation of the respective expanded (k=2) uncertainties $U(T_{nom})$ [5, 28, 29].

Table 2: Materials used for temperature calibration. T_{nom} ... nominal melting temperature, $U(T_{nom})$... uncertainty of the nominal melting temperature.

Calibration material	T_{nom} [°C]	$U(T_{nom})$ [°C]
Indium (In)	156.6	0.2
Tin (Sn)	231.9	0.2
Bismuth (Bi)	271.6	0.2
Lead (Pb)	327.5	0.2
Zinc (Zn)	419.5	0.2
Aluminium (Al)	660.3	0.2
Silver (Ag)	961.8	0.2
Gold (Au)	1064.2	0.2
Iron-Carbon eutectic (Fe-C)	1153.0	2.0
Nickel-Carbon eutectic (Ni-C)	1329.0	2.0
Nickel (Ni)	1455.0	0.2

Temperature calibration was performed in Pt crucibles with Al_2O_3 inserts and Pt lids using up to ten reference materials from Table 2. Whenever possible, the same crucible set was used. Specimens with low mass (mostly between 10 mg and 40 mg) were chosen because they produce a sharper melting peak with less onset temperature uncertainty. For the eutectic systems Fe-C and Ni-C, the metal sample was placed on a thin graphite disc within the crucible. All calibrations were conducted with heating rates of 20 K/min, 10 K/min, 5 K/min, and 2 K/min and maximum temperatures of approx. 20°C above the respective melting points. An isothermal phase was added after each dynamic heating to ensure complete melting and stabilization of the DSC signal before cooling. Prior to

the first calibration cycle, all materials were heated above their melting point once in order to form a constant contact surface with the crucible.

The effects of helium as purge gas on the calibration constant ΔT was investigated and compared to prior temperature calibrations in an argon atmosphere, both using a constant flow rate of 100 ml/min. Fig.8 shows ΔT as a function of temperature determined with the DSC 404 at a heating rate of 20 K/min.

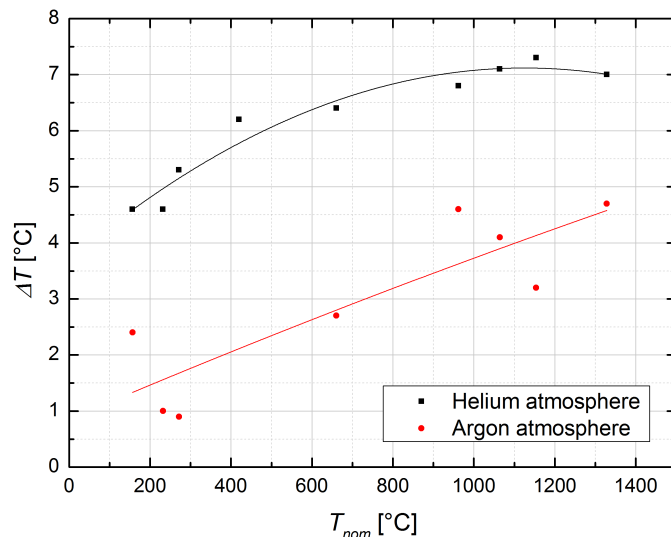


Figure 8: Influence of purge gas on temperature calibration constant ΔT measured using the DSC 404 and a heating rate of 20 K/min

The calibration materials used are shown as data points at their respective nominal melting temperatures. Nickel (with a melting temperature of 1455°C) was initially used for calibration, but subsequently discarded due to specimen oxidation which resulted in a reduced melting temperature of approx. 15°C. A second order fit was applied to cover the entire temperature range. In an argon atmosphere, the calibration factor ΔT_{Ar} increased with temperature and can be approximated by the quadratic function

$$\Delta T_{Ar} = 0.8540 + 0.0031 \cdot T_{nom} - 0.2129 \cdot 10^{-6} \cdot T_{nom}^2 \quad (18)$$

The average deviation of single calibration points from the fit generally exceeded the estimated uncertainties for the nominal melting temperatures $U(T_{nom})$ and can be used as a lower limit for the total uncertainty from temperature calibration at the respective points. This uncertainty, however, does not include other factors of influence such as thermal gradients within the calibration sample [33]. For a more thorough temperature

uncertainty evaluation, several more temperature calibration cycles using the same DSC setup need to be performed.

In a helium atmosphere, the correction ΔT_{He} increased by approx. 3°C as compared to an argon atmosphere. After an initial increase with temperature, ΔT_{He} remained rather constant above 900°C and can be approximated by the quadratic function

$$\Delta T_{He} = 3.7036 + 0.0061 \cdot T_{nom} - 2.6983 \cdot 10^{-6} \cdot T_{nom}^2 \quad (19)$$

This behavior could be attributed to the much higher thermal conductivity of helium compared to argon ($0.151 \text{ Wm}^{-1}\text{K}^{-1}$ vs. $0.018 \text{ Wm}^{-1}\text{K}^{-1}$) which would result in greater heat exchange between the crucibles and the furnace. The average deviation of single calibration points from the fit was lower in a helium atmosphere, however, only one temperature calibration was performed for each purge gas and uncertainty results can not be considered statistically significant.

Additionally, temperature calibration was performed with sapphire spacers and helium as purge gas. Its influence can be seen in Fig. 9 that compares measured offsets with ($\Delta T_{He,w/}$) and without ($\Delta T_{He,w/o}$) the use of sapphire spacer discs at a heating rate of 20 K/min.

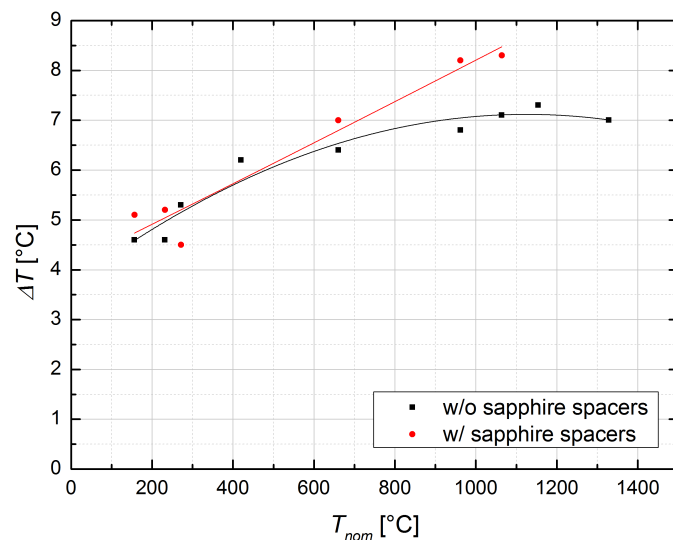


Figure 9: Influence of sapphire spacer discs on temperature calibration constant ΔT measured using the DSC 404 at a heating rate of 20 K/min

At temperatures below approx. 600°C, the difference between the temperature corrections was found to be minimal and lies well within the measurement uncertainty. Above 600°C, however, $\Delta T_{He,w/}$ increased with rising temperature, whereas $\Delta T_{He,w/o}$ remained

constant and showed a slight decline close to the maximum operating temperature of the DSC. The fitted curve with sapphire spacers was approximated by

$$\Delta T_{He,w/} = 4.1061 + 0.0040 \cdot T_{nom} + 0.0781 \cdot 10^{-6} \cdot T_{nom}^2 \quad (20)$$

Due to sample impurities and oxidation, only a limited number of calibration materials were used for calibration with sapphire spacer discs excluding the carbon eutectics and nickel.

At heating rates below 20 K/min, the correction remained similar, showing deviations of less than 1°C which is mostly within the temperature uncertainty (see Fig. 10).

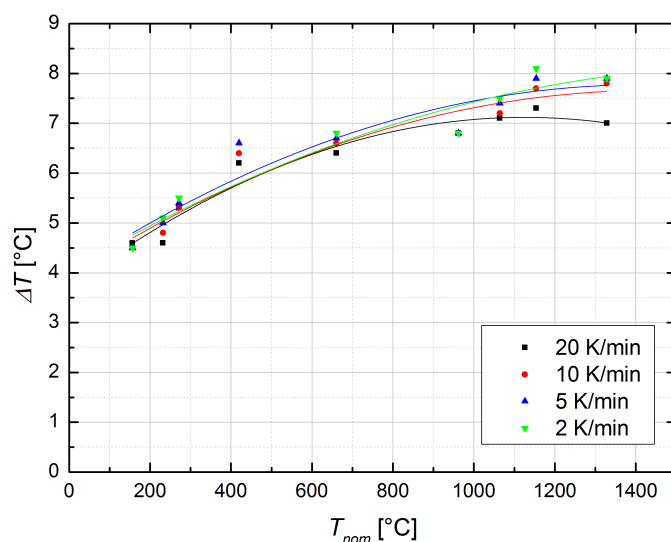


Figure 10: Influence of applied heating rates on temperature calibration constant ΔT measured using the DSC 404 in a helium atmosphere

Temperature calibration in the cooling mode was performed using the same materials from Table 2. However, due to the high purity of the calibration materials, supercooling was observed repeatedly and the solidification points of most samples were at significantly lower temperatures than the respective melting points. Thus, no meaningful calibration factor could be determined. More information about temperature calibration in the cooling mode is provided by Martins and Cruz-Pinto [6] and Malheiro et al. [38]. For more information about supercooling and the observed effect, see chapter 4.9.10 (p. 69).

Temperature calibration performed on the DSC 404 C provided results similar to the DSC 404. Fig. 11 shows the influence of sapphire spacers on the correction ΔT in a helium atmosphere using the DSC 404 C.

At low temperatures, the correction constant without sapphire spacers $\Delta T_{He,w/o}$ was

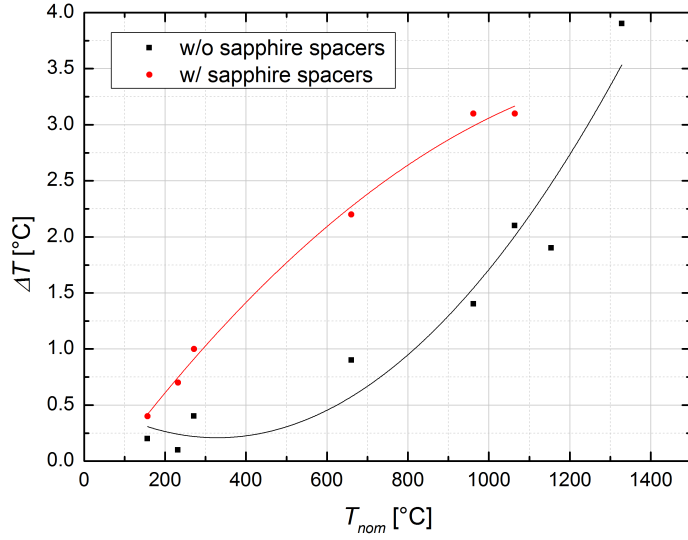


Figure 11: Influence of sapphire spacer discs on temperature calibration constant ΔT measured using the DSC 404 C and a heating rate of 20 K/min

found to be below 1°C and much smaller than the corresponding correction for the DSC 404. However, its slope increased with rising temperature up to a temperature offset of 3.9°C at 1328°C. It can be approximated by the quadratic function

$$\Delta T_{He,w/o} = 0.5688 - 0.0022 \cdot T_{nom} + 3.3278 \cdot 10^{-6} \cdot T_{nom}^2 \quad (21)$$

The use of sapphire spacer discs resulted in an only slightly elevated offset ΔT_w depending on the temperature. It is given by

$$\Delta T_{He,w/} = -0.3265 + 0.0050 \cdot T_{nom} - 1.6106 \cdot 10^{-6} \cdot T_{nom}^2 \quad (22)$$

The deviations of the individual measurements from the fit are similar to the DSC 404 and can again only provide a lower limit for the total temperature uncertainty. The influence of different heating rates for the DSC 404 C is shown in Fig. 12.

Differences between the measured corrections were also found to be low. In order to increase statistical significance, however, more calibration measurement series should be performed.

Overall, all temperature calibrations showed an increase in the correction ΔT with temperature, the only exception being the measurement without sapphire spacers and a helium atmosphere at high temperatures using the DSC 404. The selection of the purge gas had a large influence as helium increased the calibration factor by up to 4°C

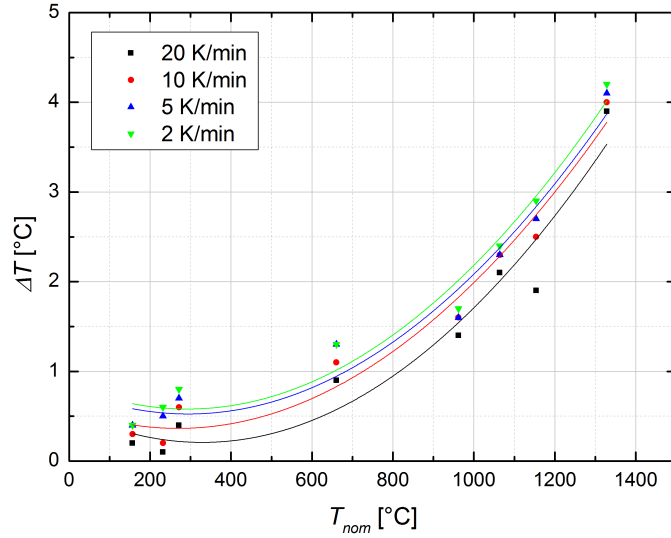


Figure 12: Influence of applied heating rates on temperature calibration constant ΔT measured using the DSC 404 C at a helium atmosphere

in comparison to argon. Sapphire spacer discs placed underneath the crucibles resulted in only minimal deviations of ΔT at low temperatures, but showed an increase up to approx. 2°C at medium and high temperatures. A lower limit for the uncertainty of the temperature at calibration points is given by their deviation from the fitted curve, and data suggests a slightly lower uncertainty when helium is used as purge gas.

4.5 Heat calibration

Heat calibration according to chapter 2.5 (p.11) was performed in order to find the temperature-dependent sensitivity coefficient that is required for quantitative characterization of transition heats. Similar to temperature calibration, heat calibration is conducted by heating reference samples with known mass m_S and nominal specific enthalpy of fusion H_{nom} above their melting point and recording the resulting DSC curve. The area A_S under the sample melting peak must be equal to the total melting enthalpy times the temperature-dependent sensitivity coefficient $k(T)$, resulting in

$$k(T) = \frac{A_S}{H_{nom} \cdot m_S} \quad (23)$$

Due to the temperature dependence of $k(T)$, this relationship is strictly only valid at the recorded melting temperatures. To extend the sensitivity coefficient across the entire temperature range, a second-order interpolation is applied. Compared to temperature calibration, suitable materials for heat calibration are further restricted since the

specimen mass must be precisely known and must not change during the measurement. Calibration substances such as zinc are difficult to use due to their tendency to evaporate at high temperatures. Other materials such as silver could not be removed from the Al_2O_3 insert, thereby preventing exact mass determination after melting. Materials used for heat calibration and their respective nominal melting temperatures T_{nom} , measured masses m_S , and nominal specific heats of fusion H_{nom} (provided by the Netzsch Proteus Measurement 6.0.0 software) including the corresponding expanded ($k=2$) uncertainties $U(m_S)$ and $U(H_{nom})$ are shown in Table 3.

Table 3: Materials used for heat calibration. T_{nom} ... nominal melting temperature, m_S ... sample mass, $U(m_S)$... uncertainty of the sample mass, H_{nom} ... nominal melting enthalpy, $U(H_{nom})$... uncertainty of the nominal melting enthalpy.

Calibration material	T_{nom} [°C]	m_S [mg]	$U(m_S)$ [mg]	H_{nom} [J/g]	$U(H_{nom})$ [J/g]
Indium (In)	156.6	22.150	0.007	28.6	0.1
Tin (Sn)	231.9	23.504	0.007	60.5	0.1
Bismuth (Bi)	271.6	18.643	0.007	53.1	0.1
Lead (Pb)	327.5	19.610	0.007	23.0	0.1
Aluminium (Al)	660.3	8.971	0.006	397.0	0.1
Gold (Au)	1064.2	43.798	0.008	63.7	0.1
Nickel (Ni)	1455.0	11.444	0.006	290.4	0.1

Heat calibration was conducted with the same measurements used for temperature calibration. For more information about the measurement setup, including utilized crucible sets and reference samples, see chapter 4.4 (p. 32). The enthalpy of fusion was measured by determining the peak area under the melting curves using the Netzsch Proteus Thermal Analysis software. A linear connection between the onset and offset of the melting peak was used as the baseline. The sensitivity coefficient was determined with equation (23), specimen mass was measured with the Sartorius MC 5 microbalance, and nominal specific enthalpy of fusion values were taken from the Netzsch Proteus Thermal Analysis software. Sensitivity coefficients were calculated for heating rates of 20 K/min, 10 K/min, 5 K/min, and 2 K/min with and without sapphire spacer discs, as well as for helium and argon as purge gases with a flow rate of 100 ml/min.

Fig. 13 shows the influence of purge gas on the measured sensitivity coefficient $k(T)$ as a function of temperature using the DSC 404 without sapphire spacer discs at a heating rate of 20 K/min. A second-order fit was applied to extend the sensitivity coefficient from the calibration points to the entire temperature range.

The sensitivity coefficient decreased substantially with increasing temperature. Starting at a value of approx. 1.00 for argon at the indium calibration point (156.6°C), it declined to approx. 0.24 at the nickel calibration point with the highest temperature of

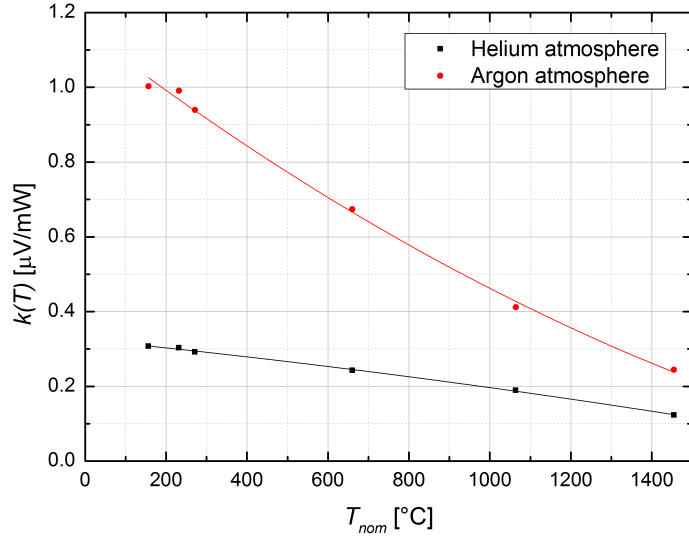


Figure 13: Influence of purge gas on sensitivity coefficient $k(T)$ measured using the DSC 404 at a heating rate of 20 K/min

1455°C. The corresponding fitted curve is given by

$$k_{Ar}(T) = 1.1516 - 8.2398 \cdot 10^{-4} \cdot T_{nom} + 1.3462 \cdot 10^{-7} \cdot T_{nom}^2 \quad (24)$$

The difference between argon and helium as purge gas was significant, and the sensitivity coefficient for helium $k_{He}(T)$ was reduced to approx. 1/3 to that of argon $k_{Ar}(T)$ at lower temperatures and 1/2 at high temperatures, and is approximated by the function

$$k_{He}(T) = 0.3253 - 1.0782 \cdot 10^{-4} \cdot T_{nom} - 0.2087 \cdot 10^{-7} \cdot T_{nom}^2 \quad (25)$$

Again, a possible explanation is the higher heat conductivity of helium which would result in additional heat flow between the crucibles through convection processes.

The influence of sapphire spacers on the sensitivity coefficient is shown in Fig. 14 using the same calorimeter in a helium atmosphere and a heating rate of 20 K/min. Compared to heat calibration without spacer discs, a slight decline in $k(T)$ was observed when sapphire spacers were utilized. The relative decrease was found to be approx. $0.3 \mu\text{V}/\text{mW}$ and is consistent throughout the entire temperature range. The fitted curve can be described by

$$k_{He,w/}(T) = 0.2955 - 0.8676 \cdot 10^{-4} \cdot T_{nom} - 0.3555 \cdot 10^{-7} \cdot T_{nom}^2 \quad (26)$$

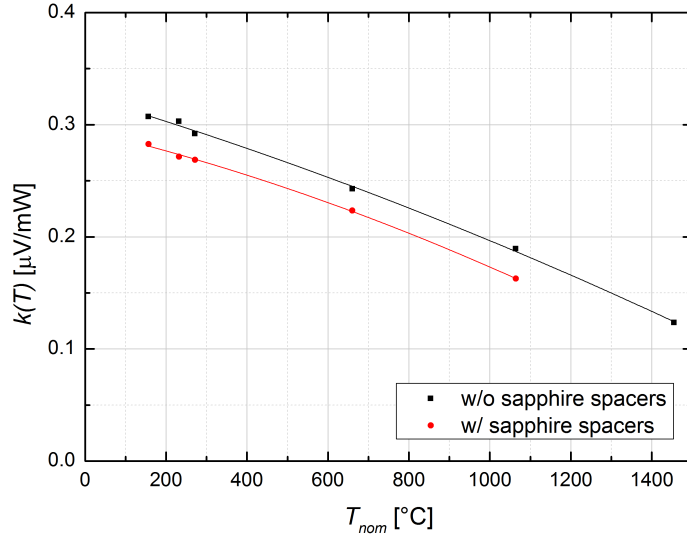


Figure 14: Influence of sapphire spacer discs on sensitivity coefficient $k(T)$ measured using the DSC 404 at a heating rate of 20 K/min

The sensitivity coefficient for different heating rates is displayed in Fig. 15. No significant dependency on the heating rate was observed.

Heat calibration performed on the DSC 404 C yielded similar results (see Fig. 16). The recorded sensitivity coefficient without sapphire spacer discs in a helium atmosphere was slightly higher as compared to the DSC 404 ranging from $0.39 \mu\text{V}/\text{mW}$ to $0.15 \mu\text{V}/\text{mW}$. The second-order fitted curve is given by

$$k_{He,w/o}(T) = 0.4154 - 2.3061 \cdot 10^{-4} \cdot T_{nom} + 3.0598 \cdot 10^{-8} \cdot T_{nom}^2 \quad (27)$$

When sapphire spacers were utilized, $k(T)$ decreased by approx. $0.5 \mu\text{V}/\text{mW}$ to $0.3 \mu\text{V}/\text{mW}$ depending on the temperature and it can be described by

$$k_{He,w/}(T) = 0.3541 - 1.3467 \cdot 10^{-4} \cdot T_{nom} - 2.7341 \cdot 10^{-8} \cdot T_{nom}^2 \quad (28)$$

All heat calibrations performed showed a decrease in the sensitivity coefficient $k(T)$ with increasing temperature. The purge gas had a large influence on $k(T)$, as argon almost tripled the sensitivity coefficient compared to helium. The usage of argon is therefore recommended for measurements of transition heats due to the higher signal strength and lower corresponding relative uncertainties. A significant, although smaller, contri-

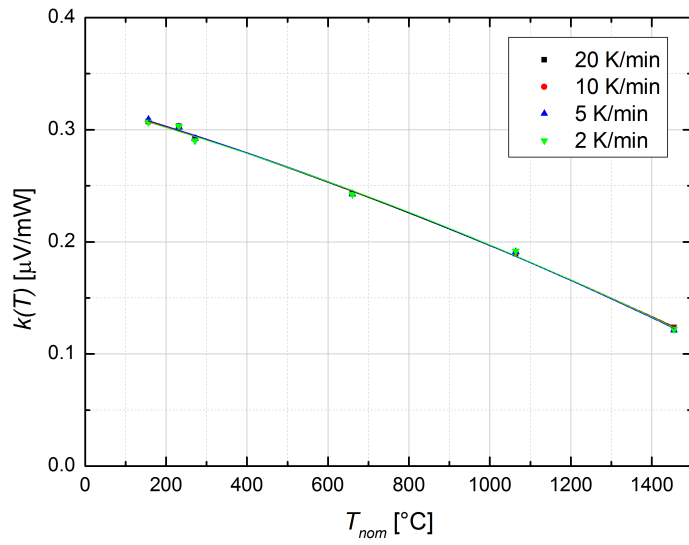


Figure 15: Influence of applied heating rates on sensitivity coefficient $k(T)$ measured using the DSC 404 in a helium atmosphere

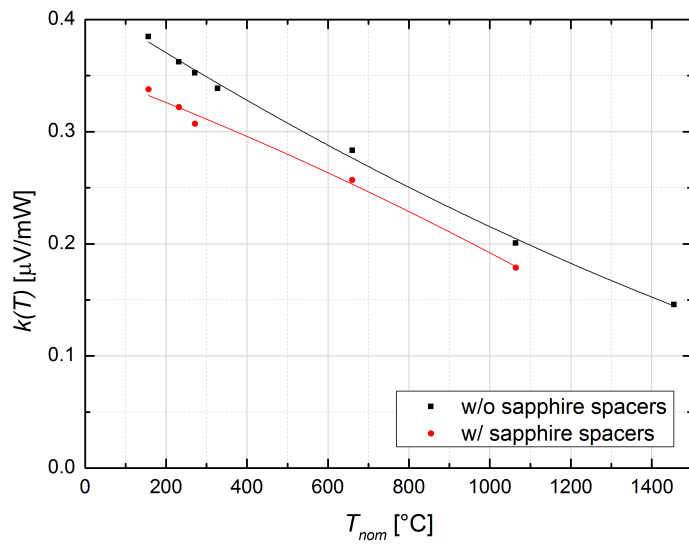


Figure 16: Influence of sapphire spacer discs on sensitivity coefficient $k(T)$ measured using the DSC 404 C and a heating rate of 20 K/min

bution originated from sapphire spacer discs as $k(T)$ decreased by approx. $0.3 \mu\text{V}/\text{mW}$ for both the DSC 404 and the DSC 404 C when sapphire spacers were used. The uncertainty $U(k(T))$ of the sensitivity coefficient remained similar for all measurements, and its lower limit at calibration points is given by the deviation from the fitted curve.

4.6 Heat flow calibration

As described in chapter 2.5 (p. 11) and chapter 4.2 (p. 29), heat flow calibration is often done separately for each sample measurement to reduce calibration error. By using the working equation (see Eq. (15) and (16), p. 29) the calibration run can then directly be compared to the sample measurement. Synthetic sapphire ($\alpha\text{-Al}_2\text{O}_3$) is typically used as calibration material due to its well-known and well-reproducible heat capacity over the entire temperature range of the DSC. Other common calibration materials are copper - which can not be used for high-temperature DSC due to its low melting point - and molybdenum. Since molybdenum reacts with trace amounts of oxygen at high temperatures and shows formation of an oxide layer on the sample surface, platinum was investigated as a possible alternative for high-temperature heat flow calibration.

In order to compare molybdenum and platinum as calibration materials, their specific heat capacities were measured by using a known synthetic sapphire reference sample which has been used extensively in prior measurements and showed no signs of deviation from its nominal properties. The resulting heat capacities for molybdenum and platinum were then compared to their respective literature values. All measurements were performed with a heating rate of $20 \text{ K}/\text{min}$ and a purge gas flow rate of $100 \text{ ml}/\text{min}$.

A rod-shaped molybdenum sample, SRM 781, was purchased from NIST (National Institute of Standards and Technology, USA), and was subsequently cut into cylindrical pieces suitable for DSC measurements. The sample used for all measurements is sized $5.2 \times 0.5 \text{ mm}$ ($d \times h$) and has a mass of $(111.086 \pm 0.012) \text{ mg}$. Due to its usage as a standard reference material, heat capacity data is provided by NIST for a wide range of temperatures [40]. The platinum and the sapphire reference sample were provided by Netzsch and have dimensions of $5.2 \times 0.5 \text{ mm}$ ($d \times h$) and $5.2 \times 1.0 \text{ mm}$ ($d \times h$), and masses of $(214.46 \pm 0.02) \text{ mg}$ and $(84.965 \pm 0.008) \text{ mg}$, respectively. Literature data for the temperature-dependent heat capacity of platinum was taken from MacLeod for temperatures below approx. 330°C and from Seville for higher temperatures [41, 42].

Fig. 17 shows the measured heat capacity c_p of the molybdenum and the platinum sample, and the respective reference values. The measurements were taken with the DSC 404 in an argon atmosphere within a timeframe of 48 hours and the ASTM working equation was used for c_p calculation. The determined heat capacity $c_{p,Mo}$ for molybdenum matches the literature data within approx. $\pm 3\%$ for temperatures above 100°C . Although increased signal noise is visible above 700°C , the measured values remain in agreement with the reference data. The platinum measurement, however, shows an increased $c_{p,Pt}$ of approx. 10% to 15% throughout the entire temperature range above 200°C as compared to literature data.

The measured heat capacity of the molybdenum reference sample decreased by approx. 5% when sapphire spacer discs were utilized (see Fig. 18), however, the average

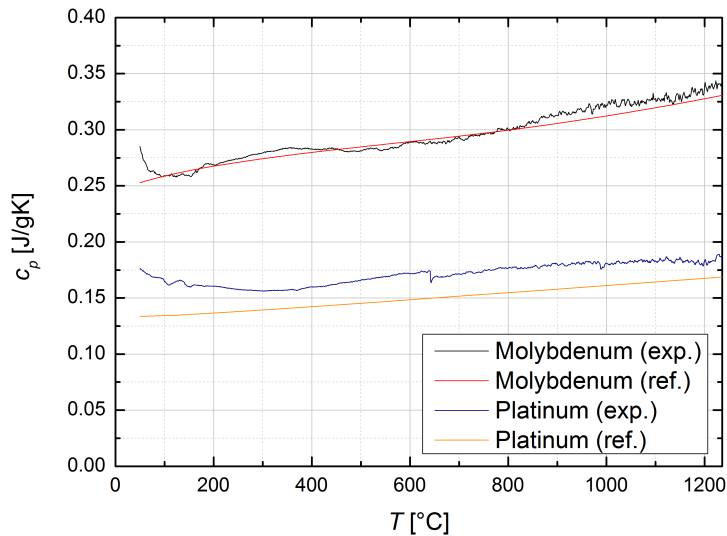


Figure 17: Heat capacities of reference materials molybdenum and platinum measured with the DSC 404 using sapphire reference

deviation from literature data did not change considerably. Similar to the measurement without sapphire spacers, the measured values did not fit literature data at temperatures below 100°C. Without further investigation, heat flow measurements in that temperature range should therefore be used carefully and with lower heating rates as uncertainty in heat capacity due to calibration might be increased.

All measurements were subsequently repeated using the DSC 404 C to investigate calorimeter-specific deviations from literature data. However, the molybdenum samples showed signs of oxidation after the measurement, and the data had to be discarded. For more information about oxidation after using the DSC 404 C, see chapter 4.9.8 (p.67) and chapter 4.9.9 (p.68).

Fig. 19 shows the influence of sapphire spacer discs on the measured heat capacity of the platinum reference sample using the sapphire specimen as the calibration reference. Both measurements were taken within 48 hours to minimize external uncertainty contributions. Favorable alignment of the measured heat capacities with the literature data can be seen at temperatures below approx. 600°C. At higher temperatures, however, the measured values are decreased by up to 10% as compared to the reference. Usage of sapphire spacer discs generally resulted in a higher measured c_p and thus in decreased deviation from literature data at high temperatures. Compared to the DSC 404, heat flow calibration measurements on the DSC 404 C show better data alignment at temperatures below 200°C.

Overall, molybdenum reference sample measurements showed better agreement with the literature data than platinum measurements, especially when the DSC 404 was

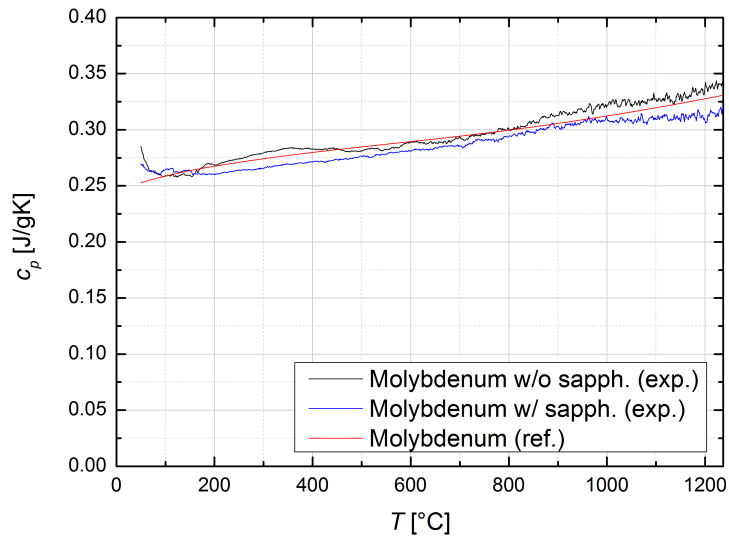


Figure 18: Heat capacities of reference material molybdenum with and without sapphire spacer discs measured with the DSC 404 using sapphire reference

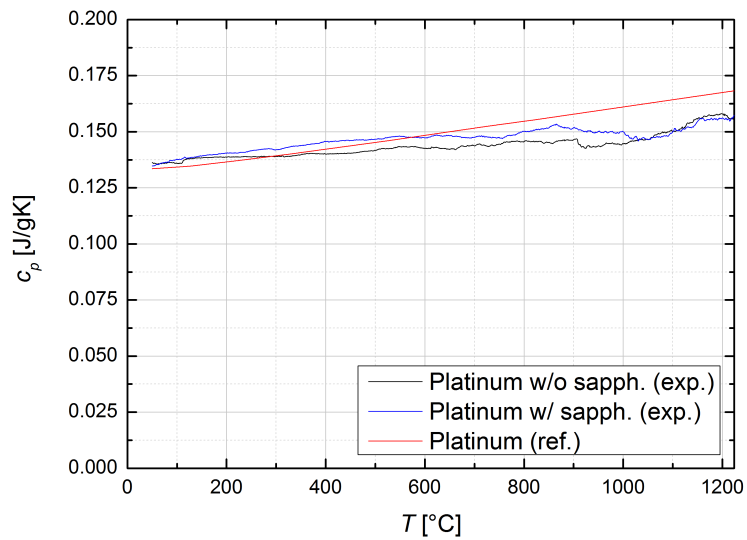


Figure 19: Heat capacities of reference material platinum with and without sapphire spacer discs measured with the DSC 404 C using sapphire reference

utilized. An average absolute deviation of less than 5% from the reference values determined by using synthetic sapphire as a reference sample makes molybdenum suitable for heat flow calibration across the entire temperature range of the DSC above 100°C. However, molybdenum is prone to oxidation at high temperatures and after each measurement it must be ensured that no oxidation layer has formed on the specimen surface. Sapphire spacer discs had little effect on the calibration measurement and can be used when needed. Platinum reference sample measurements showed deviations of up to 15% (DSC 404) and 10% (DSC 404 C) from the literature data and therefore more measurements should be conducted to provide a more detailed heat flow calibration evaluation for platinum as a calibration material.

4.7 Repeatability

Three consecutive DSC runs need to be performed for any heat capacity measurement using the working equation (see chapter 4.2, p. 29). To specify the total measurement uncertainty, the nominal uncertainties of the sample and reference masses m_S and m_R , the reference specific heat capacity $c_{p,R}$, and the uncertainty of the measured DSC signals for the baseline Φ_0 , the reference sample Φ_R , and the sample Φ_S are used. The uncertainties $U(m_S)$ and $U(m_R)$ of the specimen masses, and $U(c_{p,R})$ of the reference heat capacity are easily found by determining the nominal measurement uncertainty of the microbalance and literature research, respectively. $U(\Phi_0)$, $U(\Phi_R)$, and $U(\Phi_S)$, however, must be quantified by experiment and are dependent on the calorimeter, the crucibles and purge gas utilized, the applied temperature program, etc. As most systematic errors in c_p measurements will cancel themselves out due to baseline subtraction, the baseline stability defines the measurement repeatability (or type A uncertainty of the DSC measurement; see chapter 3.1, p. 13) which is used to evaluate the influence of the DSC signal on total uncertainty.

Typically, a single DSC run for heat capacity determination lasts 4 to 10 hours depending on the applied heating rate(s) and temperature range. Assuming the latter, a single c_p measurement takes at least 1.5 days if all runs are started during the day. To evaluate baseline stability during that timeframe, 5 consecutive runs of approx. 8 hours each were performed for each repeatability measurement resulting in a total time of 2.5 days per measurement. This was found to be a good compromise between a similar timeframe and acceptable accuracy of the evaluated uncertainty (for 5 measurements, the coverage factor of the standard deviation is approx. 36%; see chapter 3.1.4, p. 15).

Between each repeatability run, the DSC chamber was opened and the crucible (if one was utilized) was lifted from the probe holder to simulate accurate measuring conditions. Unless otherwise mentioned, all measurements were performed at a heating rate of 20 K/min, a purge gas flow rate of 100 ml/min, and were corrected with the ASTM method; see chapter 4.2 (p. 29).

4.7.1 Empty probe holder

In order to eliminate uncertainty contributions from the crucible set used, repeatability was evaluated for the "empty" probe holder. Fig. 20 shows the standard deviation ($k=1$) of the DSC signal as a function of temperature using the DSC 404. The measurement was performed in an argon and a helium atmosphere. Additionally, sapphire spacer discs with a thickness of $75\ \mu\text{m}$ were utilized to determine their influence on the total repeatability.

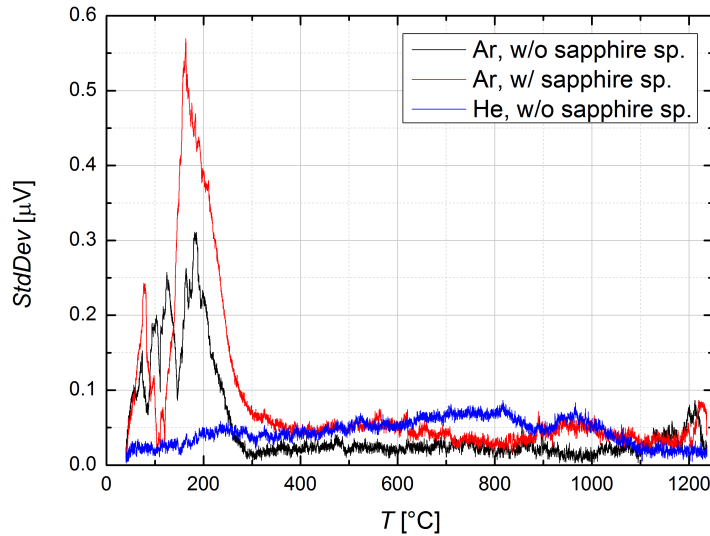


Figure 20: Repeatability without crucibles measured with the DSC 404 in an argon and helium atmosphere with and without sapphire spacer discs

It can be seen that the measured repeatability, the standard deviation of five measurements, depends strongly on the DSC setup. When argon was used as a purge gas without sapphire spacers, an increased repeatability of up to $0.30\ \mu\text{V}$ is noticeable below 300°C . At higher temperatures, repeatability is generally below $0.05\ \mu\text{V}$. A similar result was found when sapphire spacers were used, however, the initial spike is increased to approx. $0.55\ \mu\text{V}$. Repeatability in a helium atmosphere without spacer discs does not increase at low temperatures and is below $0.10\ \mu\text{V}$ throughout the entire temperature range.

Using the DSC 404 C, the low-temperature spike was found to be decreased to approx. $0.15\ \mu\text{V}$ in an argon atmosphere (see Fig. 21). At temperatures above 600°C , however, uncertainty increased up to $0.30\ \mu\text{V}$ for all three configurations.

Overall, the configuration without sapphire spacers with helium as purge gas resulted in the lowest repeatability for the DSC 404. As for the DSC 404 C, all measurements yielded similar results, and no configuration seemed to have a distinct advantage over

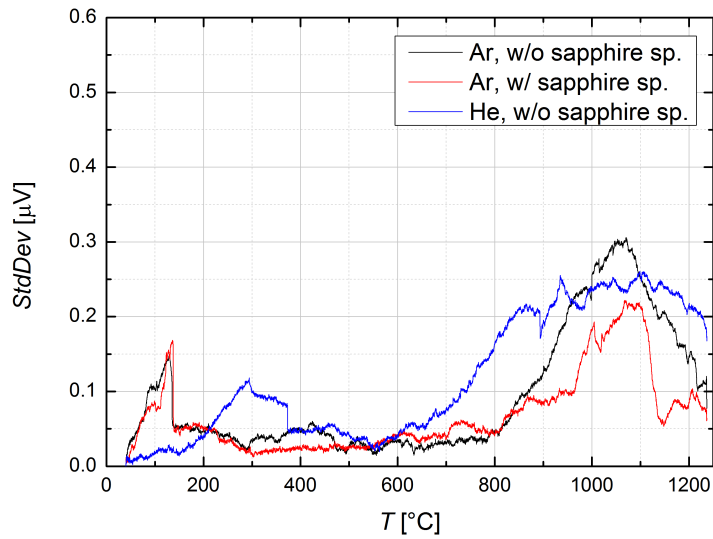


Figure 21: Repeatability without crucibles measured with the DSC 404 C in an argon and helium atmosphere with and without sapphire spacer discs

the others. Interestingly, uncertainty increased significantly for higher temperatures, whereas it remained rather constant for the DSC 404.

4.7.2 Pt crucibles with Al_2O_3 inserts

Repeatability was evaluated for three different platinum crucible sets with aluminium oxide inserts as described in chapter 4.3.1 (p.30) without a sample (baseline measurement). The three sets, labeled #4, #5, and #6 showed no signs of dents, scratching, or contamination prior to the measurement and their masses are given in Table 4.

Table 4: Platinum crucibles and aluminium oxide inserts used for repeatability measurements including their masses

Crucible set	Mass Pt pan [mg]	Mass Pt lid [mg]	Mass Al_2O_3 insert [mg]
#4 (reference pan)	175.6	89.2	50.0
#4 (sample pan)	176.4	89.0	49.1
#5 (reference pan)	177.8	87.6	47.6
#5 (sample pan)	178.7	86.6	46.1
#6 (reference pan)	173.5	82.3	49.6
#6 (sample pan)	171.5	83.9	49.7

Using the DSC 404 and an argon atmosphere, overall standard deviation for five consecutive measurements ranged from below $0.15 \mu\text{V}$ (for #5 and #6 with sapphire spacer discs) to $0.5 \mu\text{V}$ (for #5 without sapphire spacers) if the initial uncertainty peak below 300°C is disregarded (see Fig. 22). Given the results from Fig. 20 (p. 46), it is assumed that the increased uncertainty around 200°C is caused by the DSC probe holder setup rather than the utilized crucibles. At higher temperatures, however, the influence of the crucibles becomes dominant and peaks at approx. 600°C . No visible correlation was found whether sapphire spacers were utilized or not.

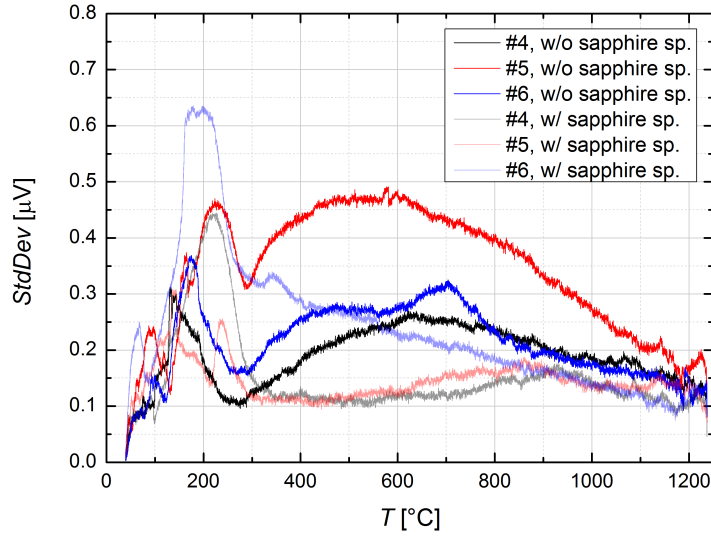


Figure 22: Repeatability of 3 different $\text{Pt}+\text{Al}_2\text{O}_3$ crucibles measured with the DSC 404 in an argon atmosphere with and without sapphire spacer discs

Fig. 23 shows that if helium was utilized as purge gas, the overall uncertainty was slightly increased as compared to an argon atmosphere. However, no initial peak was observed which matches the findings for the empty probe holder (see Fig. 20, p. 46). Uncertainty deviations between the measured pans were found to remain significant.

Compared to repeatability measurements on the DSC 404, the DSC 404 C shows similar results with an argon atmosphere (see Fig. 24). Without the initial peak observed on the DSC 404, repeatability ranged from $0.15 \mu\text{V}$ to $0.45 \mu\text{V}$ depending on the crucible set used. Differences between the crucible sets are large and do not seem to be correlated to usage of sapphire spacer discs. For example, #5, used without spacers, yielded the highest uncertainty for both the DSC 404 and the DSC 404 C, whereas #5 with sapphire spacers resulted in low uncertainty in both cases.

When helium was utilized as a purge gas, uncertainty was found to be significantly lower than in an argon atmosphere, ranging from $0.15 \mu\text{V}$ to $0.25 \mu\text{V}$ (see Fig. 25). Dif-

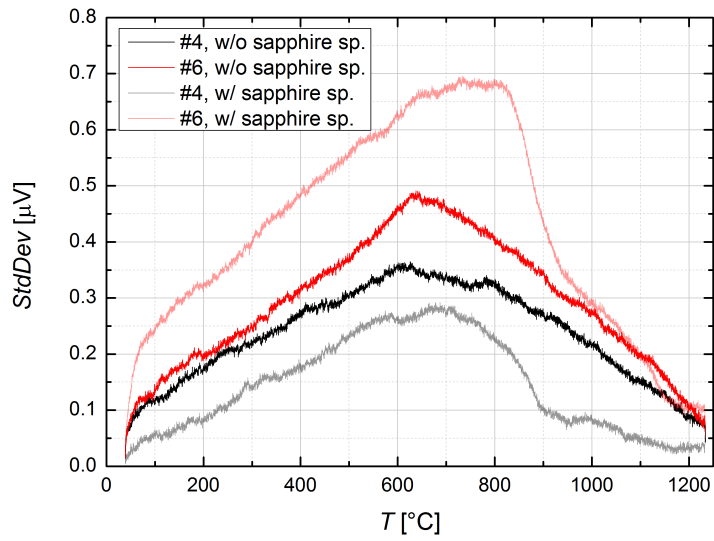


Figure 23: Repeatability of 2 different Pt+Al₂O₃ crucibles measured with the DSC 404 in a helium atmosphere with and without sapphire spacer discs

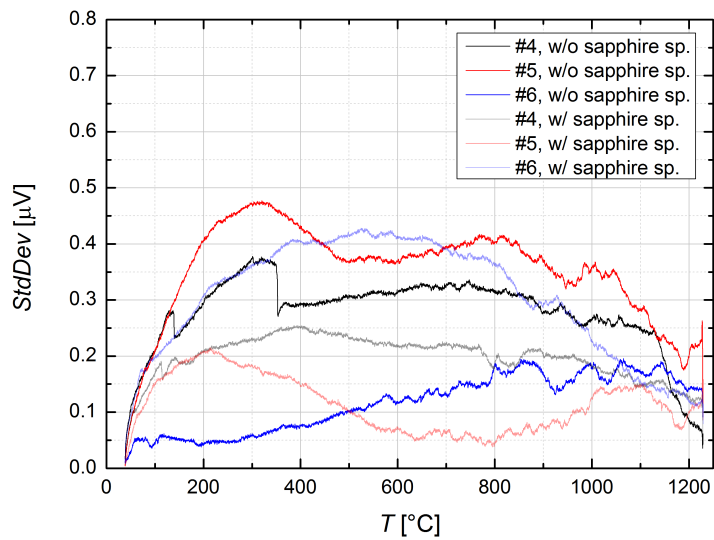


Figure 24: Repeatability of 3 different Pt+Al₂O₃ crucibles measured with the DSC 404 C in an argon atmosphere with and without sapphire spacer discs

ferences between the crucibles are smaller and sapphire spacer discs have little impact on the repeatability.

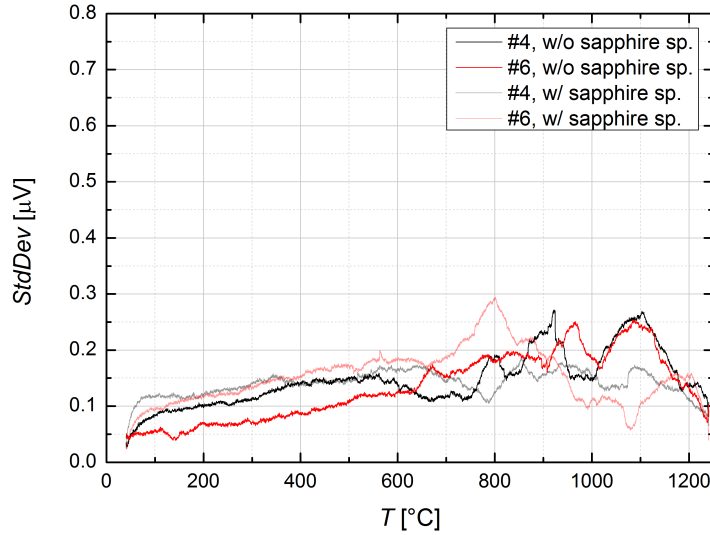


Figure 25: Repeatability of 2 different Pt+Al₂O₃ crucibles measured with the DSC 404 C in a helium atmosphere with and without sapphire spacer discs

In all cases with the exception of the combination DSC 404 C and helium as purge gas, usage of different crucible set resulted in a variation of the measured repeatability of up to 400 %. Sapphire spacer discs had no large impact on the average repeatability, however, using the same crucible set with and without spacers usually changed its characteristics considerably. The "best" set showed an average deviation of approx. 0.15 μ V for each purge gas-crucible combination which is assumed to be the lower limit for the given DSC setup.

4.7.3 Graphite crucibles

Three different graphite crucible sets were investigated as an alternative to the platinum and aluminium oxide combination (see chapter 4.3.1, p. 30). Due to possible reactions with the probe holder, they were always used with sapphire spacer discs. The masses for the graphite sets #7, #8, and #9 are given in table 5 below.

Table 5: Graphite crucibles used for repeatability measurements including their masses

Crucible set	Mass graphite pan [mg]	Mass graphite lid [mg]
#7 (reference pan)	62.8	27.3
#7 (sample pan)	62.0	27.4
#8 (reference pan)	70.1	26.0
#8 (sample pan)	66.2	27.0
#9 (reference pan)	63.1	27.2
#9 (sample pan)	62.2	26.8

All three empty graphite crucible sets were used in an argon atmosphere, and one (#9) was additionally evaluated with helium as purge gas. Measurements with the DSC 404 show average standard deviations between $0.15 \mu\text{V}$ and $0.25 \mu\text{V}$ when the low-temperature peaks are disregarded (see Fig. 26). Compared to the Pt+Al₂O₃ combination, no "high-uncertainty" crucible with a deviation above $0.3 \mu\text{V}$ was found, whereas the lower limit remains similar. Crucibles #8 and #9, measured in an argon atmosphere, show a strong temperature influence, with standard deviations ranging from $0.05 \mu\text{V}$ to $0.30 \mu\text{V}$. #9, measured in helium, features the lowest uncertainty below 250°C and above 1050°C , and lies between the argon measurements at intermediate temperatures.

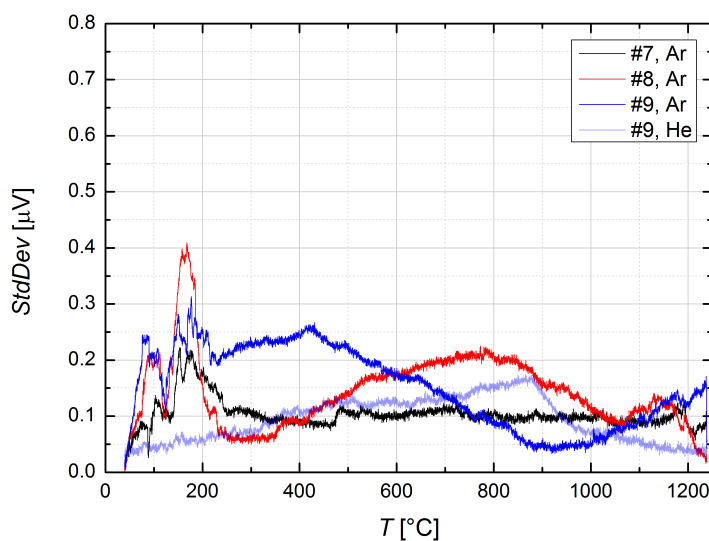


Figure 26: Repeatability of 3 different Graphite crucibles measured with the DSC 404 in an argon and helium atmosphere with sapphire spacer discs

DSC 404 C measurements can be seen in Fig. 27. Similar to the DSC 404, average standard deviations range from $0.15 \mu\text{V}$ to $0.25 \mu\text{V}$, however, they are less temperature-

dependent and remain fairly constant between 200°C and 900°C. Helium as a purge gas did not show significant improvement over argon with the DSC 404 C.

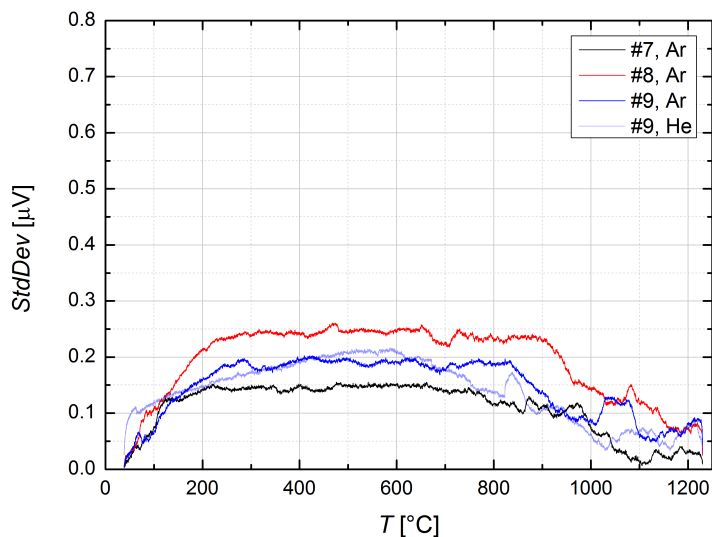


Figure 27: Repeatability of 3 different Graphite crucibles measured with the DSC 404 C in an argon and helium atmosphere with sapphire spacer discs

Compared to Pt+Al₂O₃ crucibles, Graphite pans show significant improvement in average repeatability. Whereas the "best" pan combination still results in a time-average standard deviation of approx. 0.15 μ V, there are no crucibles that exceed a total uncertainty of 0.30 μ V. Helium as a purge gas did not improve repeatability considerably and no measurement data was collected without sapphire spacer discs as the graphite pans might show reactions with the probe holder.

4.7.4 Reference samples

All prior repeatability measurements were taken with empty crucibles corresponding to baseline measurements. As two out of the three DSC runs needed for heat capacity measurements are taken with a (reference) sample, however, an additional contribution from the specimen-crucible contact might increase the uncertainty for Φ_R and Φ_S . A synthetic sapphire sample with a mass of (83.286 \pm 0.008) mg was chosen for the following repeatability measurements since it is commonly utilized as a certified reference material and very stable across the entire temperature range of the DSC.

Fig. 28 shows the repeatability of the sapphire reference sample using the DSC 404 C and 3 different crucibles made of platinum (#4 and #6) and graphite (#7) with and without sapphire spacer discs in an argon atmosphere. The average standard deviation ranges from approx. 0.2 μ V up to 0.5 μ V depending on temperature and the crucible

used. The graphite crucible features a higher deviation below 600°C as compared to the same measurement without the sapphire sample, whereas the deviation with the Pt+Al₂O₃ crucibles is slightly elevated across the entire temperature range. Overall, the increase can not be considered statistically significant due to the low number of DSC runs.

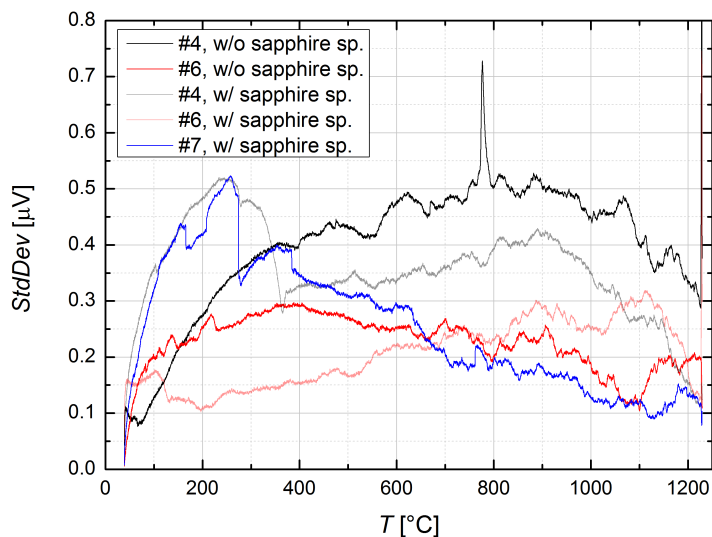


Figure 28: Repeatability of a sapphire reference sample measured in 3 different crucibles with the DSC 404 C in an argon atmosphere with and without sapphire spacer discs

The same measurement taken with helium as a purge gas shows a reduced standard deviation of all crucibles compared to an argon atmosphere (see Fig. 29). Ranging from 0.15 μV to 0.50 μV , the decrease can be considered statistically significant and is particularly visible for Pt+Al₂O₃ crucibles.

In addition to the sapphire reference sample, the molybdenum reference sample and platinum sample introduced in chapter 4.6 (p. 42) were also investigated (see Fig. 30) using the DSC 404 and Pt+Al₂O₃ crucibles without sapphire spacers in an argon atmosphere. Molybdenum features a repeatability similar to the sapphire reference sample with an average deviation of less than 0.4 μV . Platinum, on the other hand, shows a deviation increased by a factor of two, ranging from 0.25 μV to 0.90 μV . Since platinum also performed poorly at absolute heat capacity values as a heat flow calibration material (see chapter 4.6, p. 42), the deviation is thought to be attributed to sample-specific properties and does not reflect actual reference sample repeatability.

Overall, reference sample measurements showed a slightly inferior repeatability as compared to baseline measurements. The "best" crucible sets were found to have an average standard deviation of approx. 0.20 μV (0.15 μV for baseline measurements) which can be assumed to be the lower limit for $U(\Phi_R)$ and $U(\Phi_S)$.

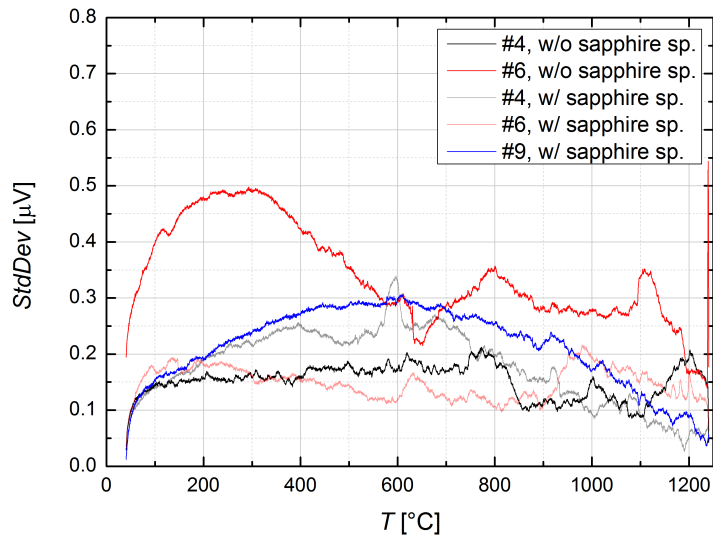


Figure 29: Repeatability of a sapphire reference sample measured in 3 different crucibles with the DSC 404 C in a helium atmosphere with and without sapphire spacer discs

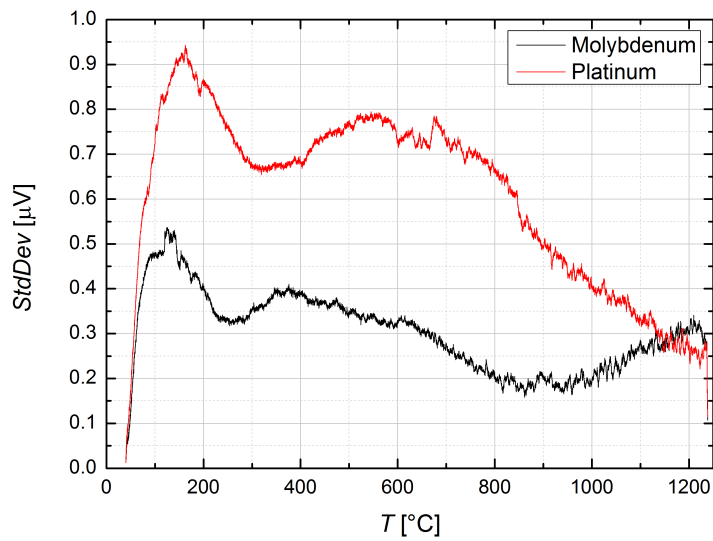


Figure 30: Repeatability of a molybdenum and a platinum reference sample measured in a Pt+Al₂O₃ crucible with the DSC 404 in an argon atmosphere without sapphire spacer discs

4.7.5 Influence of sapphire spacer discs and purge gas

For comparison, the average repeatability for Pt+Al₂O₃ crucibles as a function of temperature using the DSC 404 is given by Fig. 31. When argon was utilized as a purge gas, average standard deviations range from 0.15 μ V to 0.35 μ V and peak at approx. 700°C. Usage of sapphire spacer discs significantly reduces the deviation to below 0.20 μ V across the entire temperature range above 300°C. A helium atmosphere results in slightly increased standard deviations of up to 0.45 μ V at 700°C and sapphire spacers show little effect. The peak at approx. 200°C is limited to argon and does not occur when helium is utilized.

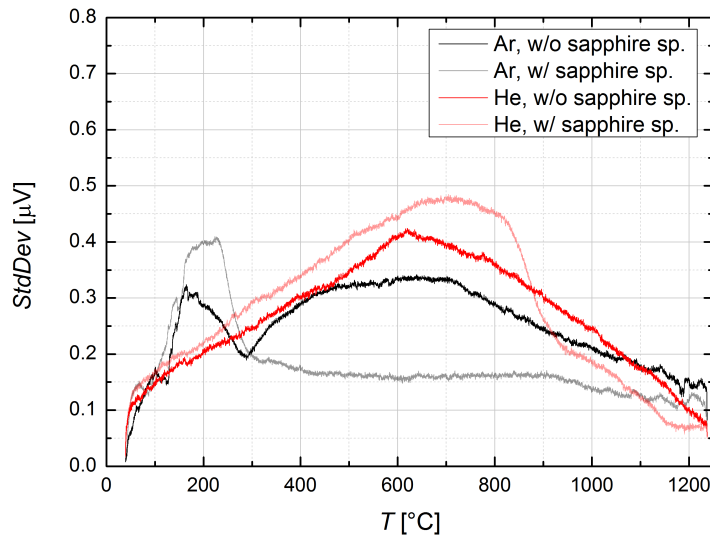


Figure 31: Average repeatability of Pt+Al₂O₃ crucibles measured with the DSC 404 in an argon and helium atmosphere with and without sapphire spacer discs

Average repeatability for the DSC 404 C is improved as compared to the DSC 404 and ranges from 0.1 μ V to 0.3 μ V (see Fig. 32). Usage of helium as a purge gas is generally favorable in repeatability measurements and decreases the average uncertainty to approx. 50% of that of argon at temperatures below 700°C. At higher temperatures, the purge gas does not contribute significantly to overall repeatability. Sapphire spacer discs had little effect on the average standard deviation.

6.7.5.1 Flow rate dependency on the DSC signal

Prior to all DSC runs a constant purge gas flow rate of 100 ml/min was set. During measurements with the DSC 404, however, the flow rate was found to steadily decrease to a final value of approx. 85 ml/min for argon and 80 ml/min for helium over the course

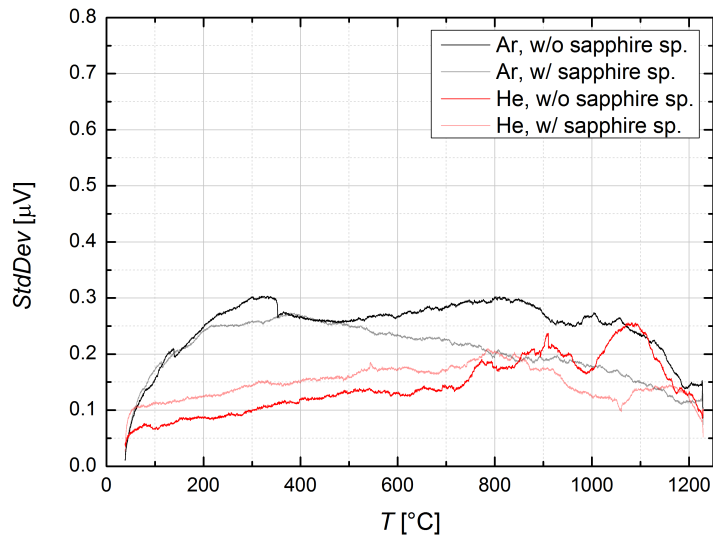


Figure 32: Average repeatability of Pt+Al₂O₃ crucibles measured with the DSC 404 C in an argon and helium atmosphere with and without sapphire spacer discs

of about one hour (see also chapter 4.9.4, p.66). As purge gas flow contributes to heat flow from and towards the crucibles, the effects of purge gas flow variations can not be neglected. They were quantified by varying the flow rate during an isothermal segment and recording the changes in the DSC signal. This procedure was then repeated for three temperature stages (400°C, 800°C, and 1200°C) and for flow rates between 50 ml/min and 300 ml/min for helium, and 50 ml/min and 100 ml/min for argon (the lower maximum flow rates for argon result due to limitations of the utilized flow rate meters). Results for the DSC 404 including the measured uncertainty given by the signal noise at the respective temperatures are shown in Fig. 33.

The DSC signal was found to deviate strongly when the flow rate of argon was modified at low temperatures. At 400°C, the signal increased by 0.25 µV when the flow rate was reduced to 75 ml/min (from the reference value of 100 ml/min), and increased by 0.52 µV when the flow rate was further reduced to 50 ml/min. Similar behaviour was observed at 800°C, with an increase to 0.17 µV (at 75 ml/min) and 0.19 µV (at 50 ml/min). At 1200°C, the DSC signal seemed to decrease for lower flow rates, however, the uncertainty at the respective points exceeds the measured values and they can not be considered statistically significant. A linear interpolation of the data shows an apparent signal change of +0.14 µV at 400°C for the lowest encountered flow rate of 85 ml/min during DSC measurements, and a signal change of +0.06 µV at 800°C. Helium does not show significant signal changes regardless of the flow rate and the temperature. Due to the observation that the flow rate only decreases for approx. one hour and then remains constant for the remainder of the measurement, the signal change for argon can be

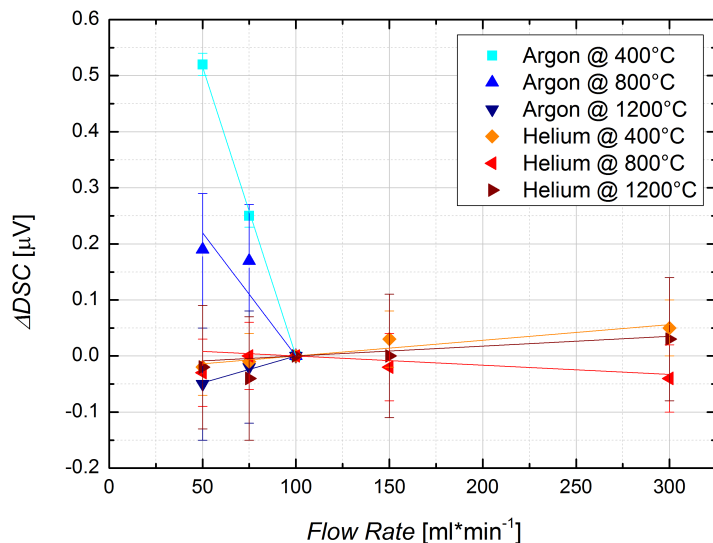


Figure 33: DSC signal changes as a function of purge gas flow rate measured with the DSC 404 at different temperatures (a flow rate of 100 ml/min is used as reference)

neglected for most measurements. However, when high-precision recordings within a short timeframe after starting are necessary, a constant purge gas flow rate must be ensured (e.g. by starting purge gas flow an hour prior to the measurement) or active adjustment is necessary.

Although the purge gas flow rate of the DSC 404 C did not vary during measurements, the influence of different flow rates on the DSC signal was determined (see Fig. 34). While argon flow rate changes did not show a significant impact, a signal decrease was found with increasing helium flow. Starting at $+0.06 \mu\text{V}$ (50 ml/min), the signal change reached $-0.10 \mu\text{V}$ (300 ml/min) at 400°C, and slightly lower absolute values at higher temperatures.

The much smaller signal change of the DSC 404 C as compared to the DSC 404 could be attributed to the location of the purge gas inlet and outlet valves. Whereas the inlet is located close to the outlet at the bottom of the DSC 404, the outlet valve of the DSC 404 C was moved to the top of the calorimeter. Overall, the only significant impact on the DSC signal results from argon flow rate changes for the DSC 404.

4.7.6 Influence of applied heating rate

As described in chapter 4.1.4 (p. 28), variable heating rates ranging between 2 K/min and 20 K/min are applied. For repeatability determination, only heating rates of 10 K/min and 20 K/min were used as evaluating all heating rates would have increased the required measurement time to unacceptable durations. Since there are a number of DSC

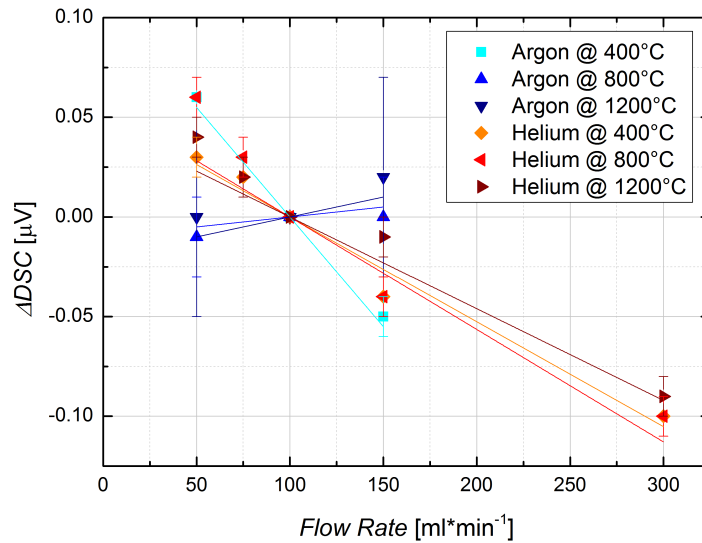


Figure 34: DSC signal changes as a function of purge gas flow rate measured with the DSC 404 C at different temperatures (a flow rate of 100 ml/min is used as reference)

applications in the cooling mode, the corresponding cooling rates were also measured to investigate the symmetry of the repeatability for heating and cooling (see also [43]).

Fig. 35 shows the average repeatability of all Pt+Al₂O₃ crucibles measured with the DSC 404 and an argon atmosphere without sapphire spacer discs for different heating rates. "Up" and "down" refers to the corresponding heating and cooling rates, respectively. It can be seen that the commonly utilized heating rate of 20 K/min results in the highest standard deviation, ranging from 0.15 μV to 0.35 μV, whereas on cooling, the repeatability is improved by approx. 30%. A heating rate of 10 K/min results in even lower deviations of less than 0.20 μV across the entire temperature range, and cooling with 10 K/min further decreases it by another 30%. No uncertainty peak at temperatures below 300°C was found in the cooling mode.

The DSC 404 C also shows reduced uncertainty for a heating rate of 10 K/min as compared to a rate of 20 K/min (see Fig. 36). However, differences between heating and cooling for both 10 K/min and 20 K/min are marginal and can not be considered statistically significant.

As it was found that a heating rate of 10 K/min results in improved repeatability when Pt+Al₂O₃ crucibles were utilized in an argon atmosphere without sapphire spacers, conducting precision measurements at decreased heating rates might be of advantage.

In addition, the DSC 404 shows significant improvement of the repeatability in the cooling mode. Due to the difficulties of conducting a precise temperature calibration on cooling (see chapter 2.4, p.10), heat capacity measurements in the cooling mode

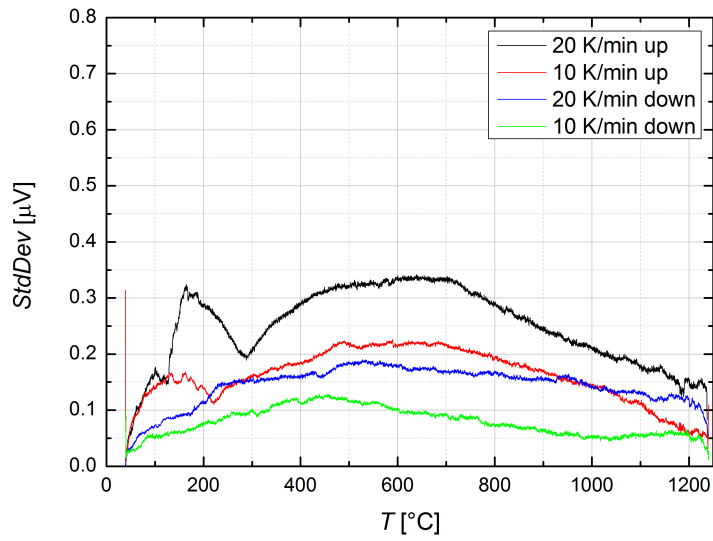


Figure 35: Average repeatability of Pt+Al₂O₃ crucibles measured with the DSC 404 in an argon atmosphere without sapphire spacer discs for two heating rates

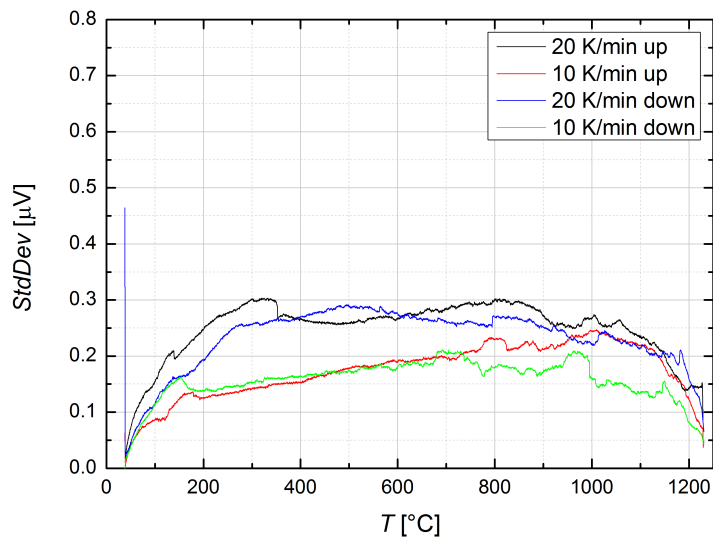


Figure 36: Average repeatability of Pt+Al₂O₃ crucibles measured with the DSC 404 C in an argon atmosphere without sapphire spacer discs for two heating rates

might result in lower total uncertainties if the sample c_p does not strongly vary with temperature.

4.7.7 Influence of working equation

The influence of the signal correction due to isothermal signal shifts (ASTM method) described in chapter 4.2 (p. 29) was evaluated and compared to the uncorrected signals used for the ratio method (RM).

Fig. 37 shows the average repeatability of Pt+Al₂O₃ crucibles measured with the DSC 404 and an argon atmosphere, and compares the uncorrected signal repeatability (RM) to the ASTM corrected data (ASTM). It is noticeable that the ASTM correction results in lower standard deviations, especially at high temperatures and when sapphire spacers were utilized.

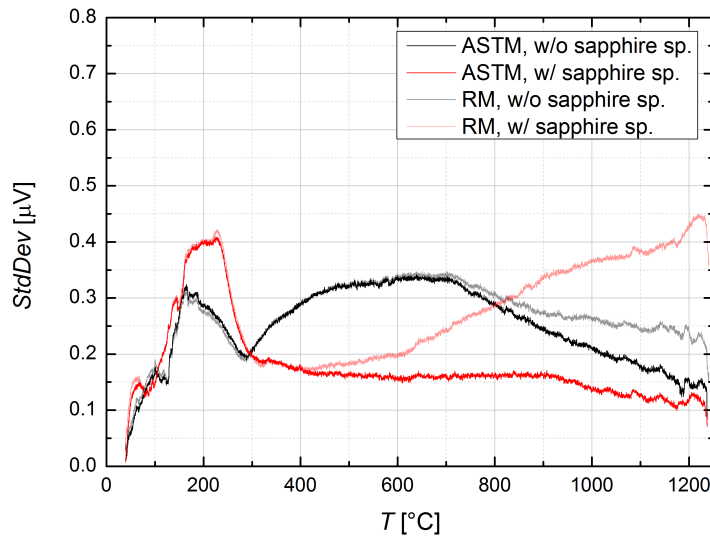


Figure 37: Influence of the used working equation on the average repeatability of Pt+Al₂O₃ crucibles measured with the DSC 404 in an argon atmosphere with and without sapphire spacers

A much smaller influence of the applied correction was found when the DSC 404 C was used (see Fig. 38). Repeatability is improved by the ASTM correction at temperatures above 900°C, however, no significant advantage is visible at low and medium temperatures. When sapphire spacers were utilized, the uncorrected signal shows decreased uncertainties below 900°C as compared to the corrected signal.

Overall, the ASTM method results in a largely improved repeatability at high temperatures and shows only little influence below 800°C (with the exception of utilizing

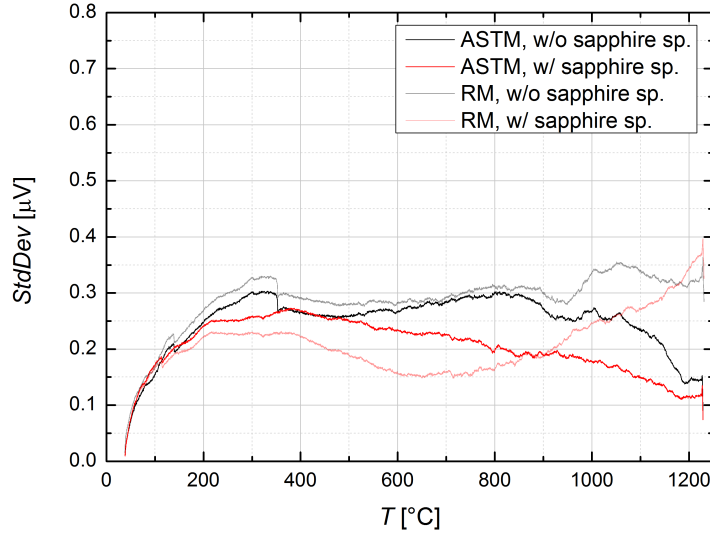


Figure 38: Influence of the used working equation on the average repeatability of Pt+Al₂O₃ crucibles measured with the DSC 404 C in an argon atmosphere with and without sapphire spacers

sapphire spacer discs with the DSC 404). Its usage is therefore recommended for all precision measurements.

4.8 Uncertainty budget

The uncertainty budget, also known as the spreadsheet model, is used to summarize all uncertainty factors of a measurement in a spreadsheet. It is particularly useful to compare the influence of input quantities with different probability distributions, determine their sensitivity coefficients, and calculate their contribution to total uncertainty.

Exemplary uncertainty budgets were calculated for a heat capacity determination of a heat-treated Nimonic 101 sample, a nickel based superalloy provided by Alstom Power Thermal Products, UK. The measurement was performed on the DSC 404 using an argon atmosphere and a Pt+Al₂O₃ crucible set. The standard deviation for the repeatability of the crucible set was assumed to be 0.15 µV across the entire temperature range for the baseline measurement, and 0.20 µV for the reference sample and sample measurements. As discussed in chapter 4.7 (p. 45), these values are estimated to form the lower limit for repeatability with the utilized DSC setup and ASTM correction (see chapter 4.2, p. 29). In order to include temperature uncertainties, the working equation was modified by introducing an additional factor $\delta T\Phi$ for each DSC run according to the subscript.

$$c_{p,S} = \frac{m_R}{m_S} \cdot c_{p,R} \cdot \frac{(\Phi_S + \delta T\Phi_S) - (\Phi_0 + \delta T\Phi_0)}{(\Phi_R + \delta T\Phi_R) - (\Phi_0 + \delta T\Phi_0)} \quad (29)$$

By using this supplementary coefficient, the temperature uncertainty can be expressed as an additional uncertainty of the DSC signal. Whereas $\delta T\Phi$ is always set to 0 as the magnitude of the signal is not altered, $U(\delta T\Phi)$ is estimated by the change in the measured signal if the temperature is varied by its given uncertainty.

To account for the temperature influence of the estimated uncertainty, the uncertainty budget was calculated at 400°C, 800°C, and 1200°C using the program GUM Workbench 1.3.6.142 by Metrodata, Germany (see Tables 6, 7, and 8, respectively). The reference sample mass and the sample mass are given by m_R and m_S , and the reference heat capacity is denoted with $c_{p,R}$. The measured signals are Φ_0 for the baseline, with $\delta T\Phi_0$ as the additional temperature factor, Φ_R for the reference sample ($\delta T\Phi_R$ being the temperature factor) and Φ_S for the sample (with $\delta T\Phi_S$ as the temperature factor).

Table 6: Uncertainty budget for a heat-treated Nimonic 101 sample at 400°C. m_R ...reference sample mass, m_S ... sample mass, $c_{p,R}$...reference sample heat capacity, Φ_0 ... baseline signal, $\delta T\Phi_0$... baseline temperature factor, Φ_R ...reference sample signal, $\delta T\Phi_R$... reference sample temperature factor, Φ_S ... sample signal, $\delta T\Phi_S$... sample temperature factor.

Quantity	Estimate	Standard uncert.	Distribution	Sensitivity coefficient	Uncertainty contribution	Index
m_R [mg]	82.286	0.005	rectangular	0.006	$28 \cdot 10^{-6}$	0.0 %
m_S [mg]	158.906	0.009	rectangular	-0.003	$-28 \cdot 10^{-6}$	0.0 %
$c_{p,R}$ [J/gK]	1.13698	0.00087	Gaussian	0.450	$390 \cdot 10^{-6}$	0.5 %
Φ_0 [μ V]	-3.9214	0.1500	Gaussian	-0.003	$-430 \cdot 10^{-6}$	0.7 %
$\delta T\Phi_0$ [μ V]	0.0000	0.0002	Gaussian	-0.003	$-430 \cdot 10^{-9}$	0.0 %
Φ_R [μ V]	26.0212	0.2000	Gaussian	-0.017	$-3.4 \cdot 10^{-3}$	41.8 %
$\delta T\Phi_R$ [μ V]	0.0000	0.0026	Gaussian	-0.017	$-45 \cdot 10^{-6}$	0.0 %
Φ_S [μ V]	21.7370	0.2000	Gaussian	0.020	$4.0 \cdot 10^{-3}$	56.9 %
$\delta T\Phi_S$ [μ V]	0.0000	0.0109	Gaussian	0.020	$220 \cdot 10^{-6}$	0.2 %
$c_{p,S}$ [J/gK]	0.51065	0.00528*	Gaussian	N/A	N/A	100.0 %

* $\cong 2.1$ % (k=2)

Table 7: Uncertainty budget for a heat-treated Nimonic 101 sample at 800°C. m_R ... reference sample mass, m_S ... sample mass, $c_{p,R}$... reference sample heat capacity, Φ_0 ... baseline signal, $\delta T\Phi_0$... baseline temperature factor, Φ_R ... reference sample signal, $\delta T\Phi_R$... reference sample temperature factor, Φ_S ... sample signal, $\delta T\Phi_S$... sample temperature factor.

Quantity	Estimate	Standard uncert.	Distribution	Sensitivity coefficient	Uncertainty contribution	Index
m_R [mg]	82.286	0.005	rectangular	0.006	$28 \cdot 10^{-6}$	0.0 %
m_S [mg]	158.906	0.009	rectangular	-0.003	$-28 \cdot 10^{-6}$	0.0 %
$c_{p,R}$ [J/gK]	1.23562	0.00087	Gaussian	0.510	$440 \cdot 10^{-6}$	0.2 %
Φ_0 [μ V]	-4.8149	0.1500	Gaussian	-0.001	$-120 \cdot 10^{-6}$	0.0 %
$\delta T\Phi_0$ [μ V]	0.0000	0.0010	Gaussian	-0.001	$-780 \cdot 10^{-9}$	0.0 %
Φ_R [μ V]	15.2215	0.2000	Gaussian	-0.032	$-6.3 \cdot 10^{-3}$	48.4 %
$\delta T\Phi_R$ [μ V]	0.0000	0.0224	Gaussian	-0.032	$-710 \cdot 10^{-6}$	0.6 %
Φ_S [μ V]	14.7362	0.2000	Gaussian	0.032	$6.5 \cdot 10^{-3}$	50.8 %
$\delta T\Phi_S$ [μ V]	0.0000	0.0025	Gaussian	0.032	$82 \cdot 10^{-6}$	0.0 %
$c_{p,S}$ [J/gK]	0.63193	0.00907*	Gaussian	N/A	N/A	100.0 %

* $\hat{=}$ 2.9 % (k=2)

Table 8: Uncertainty budget for a heat-treated Nimonic 101 sample at 1200°C. m_R ... reference sample mass, m_S ... sample mass, $c_{p,R}$... reference sample heat capacity, Φ_0 ... baseline signal, $\delta T\Phi_0$... baseline temperature factor, Φ_R ... reference sample signal, $\delta T\Phi_R$... reference sample temperature factor, Φ_S ... sample signal, $\delta T\Phi_S$... sample temperature factor.

Quantity	Estimate	Standard uncert.	Distribution	Sensitivity coefficient	Uncertainty contribution	Index
m_R [mg]	82.286	0.005	rectangular	0.006	$28 \cdot 10^{-6}$	0.0 %
m_S [mg]	158.906	0.009	rectangular	-0.003	$-28 \cdot 10^{-6}$	0.0 %
$c_{p,R}$ [J/gK]	1.29048	0.00087	Gaussian	0.550	$480 \cdot 10^{-6}$	0.0 %
Φ_0 [μ V]	-4.5917	0.1500	Gaussian	0.003	$410 \cdot 10^{-6}$	0.0 %
$\delta T\Phi_0$ [μ V]	0.0000	0.0065	Gaussian	0.003	$18 \cdot 10^{-6}$	0.0 %
Φ_R [μ V]	7.1238	0.2000	Gaussian	-0.060	$12 \cdot 10^{-3}$	52.1 %
$\delta T\Phi_R$ [μ V]	0.0000	0.0150	Gaussian	-0.060	$-900 \cdot 10^{-6}$	0.3 %
Φ_S [μ V]	7.6791	0.2000	Gaussian	0.058	$12 \cdot 10^{-3}$	47.4 %
$\delta T\Phi_S$ [μ V]	0.0000	0.0088	Gaussian	0.058	$510 \cdot 10^{-6}$	0.0 %
$c_{p,S}$ [J/gK]	0.7084	0.0168*	Gaussian	N/A	N/A	100.0 %

* $\cong 4.8$ % (k=2)

The major contribution towards uncertainty comes from the repeatability of the reference sample and sample measurement at all three evaluated temperatures, accounting to over 95 % of total uncertainty. Due to the fact that reference sample and sample signal remained very similar throughout the entire temperature range, the baseline measurement only had a minor influence on the overall uncertainty. Deviations in temperature accounted for 0.6 % or less of total uncertainty, depending on the measured temperature and slope of the DSC signal. Uncertainties contributed to the masses of reference and sample, and the reference heat capacity also had an overall influence of < 1 % and can usually be neglected.

The overall expanded (k=2) relative uncertainty for the heat capacity of the Nimonic 101 sample was found to be 2.1 % at 400°C, 2.9 % at 800°C, and 4.8 % at 1200°C. However, these values correspond to the best-case scenario which includes a large DSC signal for the reference sample and sample run, and a temperature-independent estimation of 0.15 μ V/0.20 μ V for the baseline/sample repeatability (according to chapter 4.7, p. 45). If the utilized crucibles are not selected carefully, the increased uncertainty due to repeatability will directly affect the total uncertainty. Assuming the worst-case scenario with a repeatability of 0.60 μ V and small DSC signals measured, the overall expanded (k=2) uncertainty would increase to 8 to 20 % depending on the temperature.

4.9 Sources of error

During the six-month long operation of both the Netzsch DSC 404 and the Netzsch DSC 404 C Pegasus, several problems were encountered. Some resulted in the need to repeat single measurements, while others caused the calorimeter to be out of service for extended periods of time. Whereas most incidents did not have a negative impact on the completion of this thesis and could be corrected or compensated for easily, a few malfunctions caused minor delays and will be described in more detail to prevent reoccurrence. An incomplete list is given below to provide better understanding of the instruments used and to improve troubleshooting if necessary.

4.9.1 Variations in room temperature

Changes in room temperature when using DSC can alter the measured signal significantly and should therefore be avoided. To maintain constant temperatures during the summer, air conditioning was installed in the laboratory. However, total AC power is not sufficient to maintain standard room temperature if the outside temperature exceeds 30°C. Thus, the laboratory was kept at approx. 26°C from June to July, and at slightly lower temperatures in May and August.

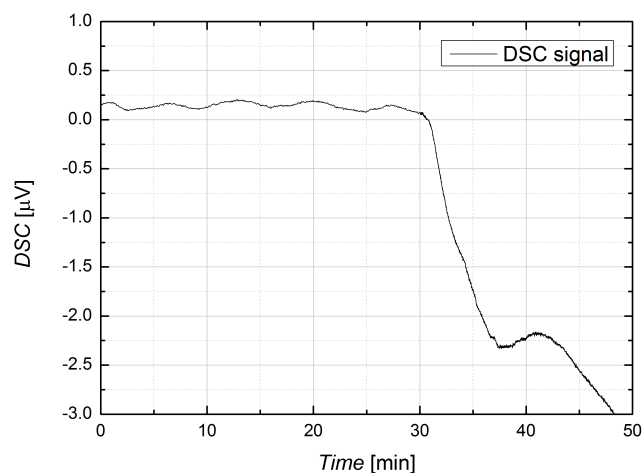


Figure 39: Influence of air conditioning on the DSC signal measured by the DSC 404

Additionally, the AC controller unit usually automatically adjusts the room temperature by switching the cooling unit on and off resulting in intermediate temperature changes of up to 1°C. These variations can be seen as an oscillation superimposed on the DSC signal, rendering precision measurements unusable (see Fig. 39). To avoid sudden temperature changes, the AC was kept running at a constant power level throughout entire measurement cycles. Careful consideration regarding the starting time/length of

the measurements and the AC fan speed used was necessary, however, to keep the room temperature as constant as possible.

4.9.2 Defective controller unit power supply

The TASC 414/2 controller unit connected to the DSC 404 abruptly stopped sending measurement data to the PC during a standard mid-temperature measurement. Following a hardware reboot, the connection to the PC was reestablished, but it disconnected again shortly after. Subsequent measurement of the controller power supply voltages showed drops in the output voltages of up to 10 %, likely causing the controller to become inoperative. Several capacitors of the power supply unit were found to be defective and were subsequently replaced, thereby restoring functionality.

4.9.3 Open purge gas inlet valve

As discussed in chapter 4.1.3 (p.26), the DSC 404 oxygen filter is connected to the measuring chamber via an inlet valve that is manually opened and closed when necessary. Upon completion of one measurement, however, the measuring chamber was opened without prior closing of the valve, resulting in air flow towards the oxygen filter. Due to the high oxygen concentration, the filter was subsequently saturated and had to be replaced.

4.9.4 Purge gas flow variations

Because heat transfer inside the DSC measuring chamber is influenced by the type and amount of purge gas used, its flow rate should be kept as constant as possible throughout the measurement. Due to reasons unknown, however, flow rate variations of up to 15 % and 20 % were observed for argon and helium, respectively. Typically, the initial flow rate would continuously decrease over the course of about one hour and then remain constant on a slightly lower level. For a more detailed analysis of the influence of purge gas flow variations, see chapter 4.7.5 (p.55) that includes a quantitative analysis. For precision measurements, purge gas flow rates should be observed and corrected for if necessary.

4.9.5 Bonding between crucibles and probe holder

During high-temperature measurements above 1200°C when using platinum pans without sapphire spacers, diffusion bonding ("sticking") between the crucibles and the probe holder can occur. It is perceived by the higher effort needed to take the pans off the holder, and is more noticeable for higher temperatures and longer measurements at these temperatures. The use of helium as a purge gas seemed to increase bonding occurrence in frequency and strength, however, the number of high-temperature measurements carried out in a helium atmosphere was not sufficient for statistical significance. Following measurements exceeding 1400°C, sticking is considerable and caution must be used as not to damage the probe holder while trying to remove the pans. Firmly gripping the pans

with suitable forceps and applying a tilting motion was found to be useful in removing strongly-bound pans from the holder. In the event that lifting with forceps is not possible, the probe holder should be removed and sudden temperature variations should be applied to its top, such as alternating baths in liquid nitrogen and boiling water. Due to rapid volume/pressure changes of the air trapped between the pans and the holder surface, the mechanical contact is subject to stress and removal could be facilitated.

In order to prevent diffusion bonding when high temperatures are required, sapphire spacers can be used. For a more detailed description including their influence on total measurement uncertainty, see chapter 4.7.5 (p. 55).

4.9.6 Crucible deformation

As discussed in chapter 3.2.1 (p. 17), inconsistent thermal contact between the crucibles and the sample holder considerably affects total repeatability. A large and constant contact surface between the sample holder and crucibles is therefore desirable, but whilst the holder surface can be assumed to be flat, the bottom of the platinum pans is subject to frequent handling and will scratch and deform over time resulting in contact loss.

A simple mechanical press consisting of a steel rod and a centering device was subsequently used to level the crucible base by applying the right amount of force with a hand-held hammer. Depending on the usage of the corresponding pans, the procedure was repeated in intervals ranging from days to months. When necessary, lids were also pressed as lid deformation can alter heat emission during measurements.

4.9.7 Sample evaporation

When subjecting specimens with high vapor pressure like zinc or manganese to high temperatures, partial or complete evaporation of the sample may occur. These samples should not be used for heat/enthalpy calibration since their exact mass during melting remains unknown. In addition, metal vapor will be deposited on the lid, thus falsifying subsequent measurements due to its added specific heat. When specimen deposition on platinum lids were encountered, they were consequently polished using a multifunction rotary tool with a grinding attachment. Partial removal of the lid material (in this case platinum) during polishing was unavoidable and resulted in lid mass loss of up to 0.3 mg. At a total mass of approx. 85 mg, these mass losses can be neglected unless polishing is conducted on a regular basis. A test measurement should always be performed following polishing to ensure total deposition removal.

4.9.8 Sample oxidation

Many materials are prone to oxidation when exposed to an oxygen-rich atmosphere at high temperatures, and thus inert purge gas such as nitrogen or argon is required during DSC measurements. In this way, most oxidation processes can be prevented, however, certain metals such as nickel were found encompassed with a thin oxidized layer upon completion of high-temperature measurements in a high-purity helium/argon

atmosphere. Because purge gas with a 5.0 purity and further oxygen removal (see chapter 4.1.3, p. 26) was utilized, this effect can be contributed to minor leaks of the inlet tubing or the vacuum-sealed measurement chamber. Throughout all measurement series, oxidation remained more noticeable when using the DSC 404 C Pegasus despite multiple checks for leakage (see chapter 4.9.9, p. 68). Therefore, sensitive samples were measured with the DSC 404.

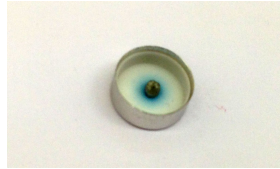


Figure 40: Nickel sample showing oxidation after being exposed to its melting temperature several times using the DSC 404 C

Oxidized samples were typically discarded since the oxidation layer can cause large variations in material properties such as melting temperature. If Al_2O_3 inserts showed signs of residue, they were thoroughly cleaned using ultrasonic baths in acetone and reused when possible.

4.9.9 Leakage

Due to recurrent specimen oxidation, two leakage checks had to be performed on the DSC 404 C Pegasus using an electronic leakage detector with a helium sniffer probe. It was found that the purge gas inlet valves showed minor signs of leakage and they were subsequently replaced. Additionally, the purge gas outlet was not appropriately vacuum-tight, yet rearward oxygen flow remains very unlikely due to the elevated pressure inside the measuring chamber. No other leakage was found.



Figure 41: DSC 404 C showing the inlet valves and the connecting purge gas line to the measuring chamber

Despite these preventative measures, sample oxidation still occurs at high temperatures. Further investigation should be conducted to find and fix the leak in order to restore full functionality.

4.9.10 Supercooling

Supercooling describes the cooling of a liquid below its freezing point without it becoming a solid and is supported by the absence of seed crystals or nuclei that can cause the liquid to crystallize around them. Due to the high purity of most samples used in DSC measurements combined with fast cooling rates, several metals will show supercooling during high temperature measurements that result in large differences between their melting and solidifying points. For example, nickel has a melting point of 1455°C , however, measurements involving subsequent melting and freezing show supercooling down to approx. 1340°C (see Fig. 42) depending on the applied cooling rate.

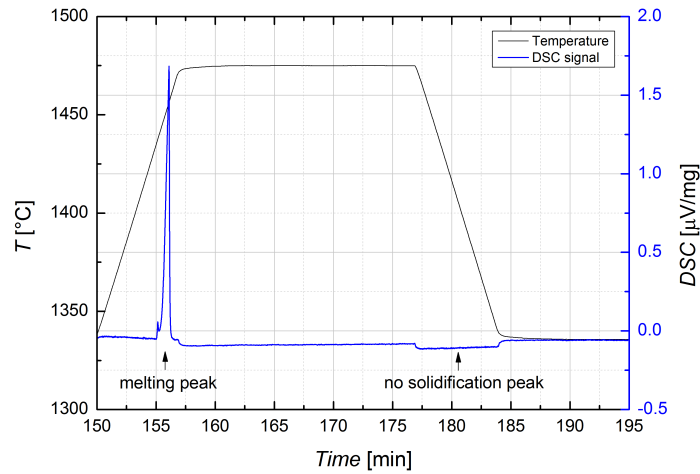


Figure 42: Nickel sample showing supercooling during temperature calibration in the cooling mode. No solidification peak can be found during the cooling phase.

The effects of supercooling are further explained by Martins and Cruz-Pinto [6] and must be considered especially when performing temperature calibrations in the cooling mode.

5 Conclusions and outlook

The measurement uncertainty of high-temperature heat flux DSCs was determined by utilizing two calorimeters at the Graz University of Technology (TU Graz), the DSC 404, commissioned in 2000, and the DSC 404 C Pegasus, commissioned in 2013 (see chapter 4.1, p. 25).

Prior to heat capacity determination and uncertainty calculation, temperature calibration was performed using a set of standard reference materials. The correction ΔT was found to be strongly dependent on temperature, ranging from 0°C to 8°C. The influence of purge gas and various crucible combinations were evaluated and quantified. Usage of helium instead of argon and sapphire spacer discs beneath the crucibles resulted in an temperature correction increased by up to 4°C and 3°C, respectively (see chapter 4.4, p. 32).

Heat calibration was performed and a sensitivity coefficient $k(T)$ between 0.25 $\mu\text{V}/\text{mW}$ and 1.00 $\mu\text{V}/\text{mW}$ for argon, and 0.15 $\mu\text{V}/\text{mW}$ and 0.30 $\mu\text{V}/\text{mW}$ for helium was determined. Sapphire spacer discs reduced $k(T)$ by approx. 0.03 $\mu\text{V}/\text{mW}$ at all measured temperatures (see chapter 4.5, p. 37).

Additionally to synthetic sapphire ($\alpha\text{-Al}_2\text{O}_3$), a widely utilized heat flow calibration material, molybdenum and platinum reference samples were evaluated for calibration. Whereas molybdenum showed favorable results with an agreement within $\pm 4\%$ from the sapphire standard, platinum revealed deviations of up to 15% (see chapter 4.6, p. 42).

Measurement repeatability was determined for all pan and purge gas combinations for both calorimeters, showing a strong dependency on the crucible set with deviations between 0.15 μV and 0.60 μV (see chapter 4.7, p. 45). Helium usage resulted in slightly lower standard deviations on average, whereas usage of sapphire spacers increased the measurement uncertainty insignificantly. Assuming the best case scenario of 0.15 μV for baseline runs and 0.20 μV for sample/reference sample runs, an uncertainty budget of the heat capacity c_p was calculated for an exemplary Nimonic 101 sample at three temperatures. It was found that measurement repeatability accounts for more than 95% of overall uncertainty, and contributions from the reference sample/sample mass and reference sample c_p can be neglected for the most part. The relative expanded ($k=2$) uncertainty for the sample heat capacity $U(c_p)$ was determined to be 2.1% at 400°C, 2.9% at 800°C, and 4.8% at 1200°C. However, $U(c_p)$ might increase by up to 400% if unsuitable "high-uncertainty" crucibles are chosen (see chapter 4.8, p. 61).

Published information regarding DSC measurement uncertainty was summarized in chapter 3.2 (p. 16) and can be used for further evaluation.

As measurement repeatability accounts for the majority of overall uncertainty, further repeatability evaluation is recommended and can be easily carried out between sample measurements. Measurements in a helium atmosphere showed promising results (except for transition heat measurements; see chapter 4.5, p. 37), however, due to the insufficient number of observations, the outcome is not statistical significant. As a possible alternative to argon and helium, nitrogen can be utilized as purge gas, and further research is suggested. Due to the fact that a number of sample materials can react with

the crucibles rendering them unusable, it is also recommended that aluminium pans be characterized as an inexpensive alternative to the platinum and graphite crucibles for usage at temperatures below approx. 600°C.

6 Acknowledgements

I would like to express my gratitude to the two persons who made this work possible: my thesis supervisor Prof. Gernot Pottlacher and my co-supervisor Dr. Boris Wilthan of the Institute of Experimental Physics at TU Graz. After Prof. Pottlacher suggested the topic of this thesis, he never hesitated to help when assistance was needed and encouraged me to grow as a research scientist. Dr. Wilthan introduced me to the functional principle of differential scanning calorimetry and subsequently devoted a large portion of his time to help me in my understanding by answering questions and continuing to provide unconditional support even after the end of his contract at TU Graz. Both Prof. Pottlacher's and Dr. Wilthan's invaluable aid and guidance were vital for the success of this thesis.

A special thanks of mine goes to Gordon McColvin of Alstom, UK, who donated the cast alloy bar for use in the EMRP project and to Lindsay Chapman of the National Physical Laboratory, UK, for permission to use the collected data of the Nimonic sample.

I also wish to thank Alexander Schmon, Kirmanj Aziz, and Thomas Macher of the Institute of Experimental Physics for their assistance with all types of technical problems, Martin Luckabauer of the Institute of Materials Physics for providing additional laboratory facilities, and Margaret R. Starcher of the Institute of Environmental Biotechnology for revisions and editing.

Last but not least I would like to express my thanks to my family and friends for their constant support and help.

References

- [1] E. S. Watson and M. J. O'Neill, "Differential microcalorimeter," US Patent #3263484, 1966.
- [2] W. F. Hemminger and H. K. Cammenga, *Methoden der Thermischen Analyse*. Springer-Verlag Berlin Heidelberg New York, 1989.
- [3] G. Höhne, W. Hemminger, and H.-J. Flammersheim, *Differential Scanning Calorimetry*. Springer-Verlag Berlin Heidelberg New York, 2003.
- [4] M. Richardson and N. Savill, "Temperatures in differential scanning calorimetry," *Thermochimica Acta*, vol. 12, pp. 213–220, 1975.
- [5] H. Preston-Thomas, "The international temperature scale of 1990 (ITS-90)," *Metrologia*, vol. 27, pp. 3–10, 1990.
- [6] J. Martins and J. Cruz-Pinto, "The temperature calibration on cooling of differential scanning calorimeters," *Thermochimica Acta*, vol. 332, pp. 179–188, 1999.
- [7] ASTM International, "Standard test method for temperature calibration of differential scanning calorimeters and differential thermal analyzers," E967-08, 2008.
- [8] ASTM International, "Standard test method for enthalpy measurement validation of differential scanning calorimeters," E2253-08, 2008.
- [9] D. A. Ditmars, S. Ishihara, S. S. Chang, and G. Bernstein, "Enthalpy and heat-capacity standard reference material: Synthetic sapphire ($\alpha - Al_2O_3$) from 10 to 2250K," *Journal of Research of the National Bureau of Standards*, vol. 87 (2), pp. 159–163, 1982.
- [10] S. Rudtsch, "Uncertainty of heat capacity measurements with differential scanning calorimeters," *Thermochimica Acta*, vol. 382, pp. 17–25, 2002.
- [11] K. Schönborn, "On the time lag between thermal event and measuring signal in a heat flux calorimeter," *Thermochimica Acta*, vol. 69, pp. 103–114, 1983.
- [12] S. Bell, "Measurement good practice guide no. 11. A beginner's guide to uncertainty of measurement," tech. rep., National Physical Laboratory, 1999.
- [13] Joint Committee for Guides in Metrology, "Evaluation of measurement data - Guide to the expression of uncertainty in measurement," 2010.
- [14] M. Richardson, "Quantitative aspects of differential scanning calorimetry," *Thermochimica Acta*, vol. 300, pp. 15–28, 1997.
- [15] G. della Gatta, M. J. Richardson, S. M. Sarge, and S. Stolen, "Standards, calibration, and guidelines in microcalorimetry part 2. Calibration standards for differential scanning calorimetry," *Pure Appl. Chem.*, vol. 78 (7), pp. 1455–1476, 2006.

- [16] C. Nieto de Castro, M. Lourenco, and M. Sampaio, "Calibration of a DSC: its importance for the traceability and uncertainty of thermal measurements," *Thermochimica Acta*, vol. 347, pp. 85–91, 2000.
- [17] J. E. Callanan and S. A. Sullivan, "Development of standard operating procedures for differential scanning calorimeters," *The Review of Scientific Instruments*, vol. 57 (10), pp. 2584–2592, 1986.
- [18] G. Höhne, H. Cammenga, W. Eysel, E. Gmelin, and W. Hemminger, "The temperature calibration of scanning calorimeters," *Thermochimica Acta*, vol. 160, pp. 1–12, 1990.
- [19] K. Kanari and T. Ozawa, "Errors and correction in complex heat capacity measurements by temperature modulated DSC," *Thermochimica Acta*, vol. 399, pp. 189–201, 2003.
- [20] S. M. Sarge, E. Gmelin, G. W. Höhne, H. K. Cammenga, W. Hemminger, and W. Eysel, "The caloric calibration of scanning calorimeters," *Thermochimica Acta*, vol. 247, pp. 129–168, 1994.
- [21] B. Wilthan, "Bestimmung der spezifischen Wärmekapazität von Stoffen mittels dynamischer Differenzkalorimetrie," Master's thesis, Technische Universität Graz, 2002.
- [22] E. Hanitzsch, "Modification of the conventional measuring method to determine the specific heat capacity using a Perkin-Elmer DSC 2," *Thermochimica Acta*, vol. 187, pp. 275–281, 1991.
- [23] J. Reichelt and W. Hemminger, "Unexpected problems in the calibration of heat-flux differential scanning calorimeters," *Thermochimica Acta*, vol. 69, pp. 59–70, 1983.
- [24] E. Gmelin and S. Sarge, "Temperature, heat and heat flow rate calibration of differential scanning calorimeters," *Thermochimica Acta*, vol. 347, pp. 9–13, 2000.
- [25] H. K. Cammenga, W. Eysel, E. Gmelin, W. Hemminger, G. W. Höhne, and S. M. Sarge, "The temperature calibration of scanning calorimeters. Part 2. Calibration substances," *Thermochimica Acta*, vol. 219, pp. 333–342, 1993.
- [26] S. M. Sarge, W. Hemminger, E. Gmelin, G. W. H. Höhne, and H. K. Cammenga, "Metrologically based procedures for the temperature, heat and heat flow rate calibration of DSC," *Journal of Thermal Analysis*, vol. 49, pp. 1125–1134, 1997.
- [27] S. M. Sarge, G. W. Höhne, H. K. Cammenga, W. Eysel, and E. Gmelin, "Temperature, heat and heat flow rate calibration of scanning calorimeters in the cooling mode," *Thermochimica Acta*, vol. 361, pp. 1–20, 2000.

- [28] “The international practical temperature scale of 1968. Amended edition of 1975.,” *Metrologia*, vol. 12, pp. 7–17, 1976.
- [29] Y. Yamada, H. Sakate, F. Sakuma, and A. Ono, “High-temperature fixed points in the range 1150°C to 2500°C using metal-carbon eutectics,” *Metrologia*, vol. 38, pp. 213–219, 2001.
- [30] S. C. Mraw, “Mathematical treatment of heat flow in differential scanning calorimetry and differential thermal analysis instruments,” *The Review of Scientific Instruments*, vol. 53 (2), pp. 228–231, 1982.
- [31] W. Baumann, A. Leineweber, and E. J. Mittemeijer, “Calibration and desmearing of a differential thermal analysis measurement signal - upon heating and cooling - in the high-temperature region,” *Thermochimica Acta*, vol. 472, pp. 50–54, 2008.
- [32] L. A. Chapman, “Application of high temperature DSC technique to nickel based superalloys,” *Journal of Materials Science*, vol. 39, pp. 1–8, 2004.
- [33] R. Comesaña, M. A. Gómez, M. A. Álvarez, and P. Eguía, “Thermal lag analysis on a simulated TGA-DSC device,” *Thermochimica Acta*, vol. 547, pp. 13–21, 2012.
- [34] W. Poeßnecker, “Heat losses which cannot be compensated for and their contribution to the temperature dependence of caloric measuring errors in dynamic differential calorimeters,” *Thermochimica Acta*, vol. 229, pp. 97–109, 1993.
- [35] ASTM International, “Standard practice for heat flow calibration of differential scanning calorimeters,” E968-02, 2008.
- [36] ASTM International, “Standard test method for determining specific heat capacity by differential scanning calorimetry,” E1269-11, 2011.
- [37] M. M. Hopkins, “High temperature differential thermal analysis apparatus,” *The Review of Scientific Instruments*, vol. 35 (12), pp. 1658–1661, 1964.
- [38] M. Malheiro, J. Martins, and J. C. Pinto, “Evaluation of the calibration errors on cooling of a differential scanning calorimeter using different sets of standard metals,” *Thermochimica Acta*, vol. 420, pp. 155–161, 2004.
- [39] M. J. O’Neill, “Measurement of specific heat functions by differential scanning calorimetry,” *Analytical Chemistry*, vol. 38, pp. 1331–1336, 1966.
- [40] National Bureau of Standards, “Standard reference material 781: Molybdenum - Heat capacity,” 1977.
- [41] A. C. MacLeod, “Enthalpy and derived thermodynamic functions of platinum and a platinum + rhodium alloy from 400 to 1700 K,” *J. Chem. Thermodynamics*, vol. 4, pp. 391–399, 1972.

- [42] A. H. Seville, “The heat capacity of platinum at high temperatures,” *J. Chem. Thermodynamics*, vol. 7, pp. 383–387, 1975.
- [43] S. Neuenfeld and C. Schick, “Verifying the symmetry of differential scanning calorimeters concerning heating and cooling using liquid crystal secondary temperature standards,” *Thermochimica Acta*, vol. 446, pp. 55–65, 2006.